

7. GEOLOGY

CONTENTS

7.	GEOLOGY.....	7-1
7.1	Geological Outline of the Project Area.....	7-1
7.2	Geological Investigation.....	7-2
7.2.1	Past Geological Investigations.....	7-2
7.2.2	Geological Investigation in Feasibility Stage	7-2
7.3	El Chaparral Project Area	7-6
7.3.1	Reservoir Area	7-6
7.3.2	Dam Site	7-7
7.3.3	Power Station.....	7-16
7.3.4	Construction Material	7-17
7.4	La Honda Project.....	7-23

7. GEOLOGY

7.1 Geological Outline of the Project Area

The topography of the Project Area was studied by a topographical map drawn to scales of 1:50,000 and 1:25,000, and the aerial photograph to a scale 1:33000. Some locations covered by the Project were surveyed on site.

The Torola River basin is located in the northeast of El Salvador. The mountains in this area are 500 m to 1800 m in elevation, and their ridges and slopes are gentle in general.

In the Project area, the Torola River flows westward with many meanders, and its river bed is 130 to 300 m in elevation. The drainage system is not typical except the radial pattern in the vicinity of Cacahuatique Mountain (1663 m in elevation) on the left bank of Torola River. The main stream passes some steep valleys with steep undercut slopes and narrow flat lands such as bars and terraces at the valley bottom. Only one exception is a small basin composed of low and gentle hills in the vicinity of Carolina Town. Fundamentally, gentle hills and valleys indicate underling soft rocks, while steep slopes and ridges indicate hard rocks. In addition, steep slopes may also indicate a recent rapid erosion by rivers. Many examples of the eroded slopes were observed in the undercut slopes and the slopes of V shaped valley formed by the rapid down-cutting of the main river and their tributaries, and they are distributed throughout the vicinity of Cacahuatique Mountain. Some land-slide topographies were observed in the Project Area.

The Torola River basin's foundation is composed mainly of the rocks formed by the volcanic activity in Tertiary and Quaternary Ages. The Tertiary strata are composed of volcanic and pyroclastic rocks. They are acidic-to-intermediate rocks of Morazan Formation, acidic rocks of Chalatenango Formation, and basic-to-intermediate rocks of Balsamo Formation. The Quaternary volcanic rocks are acidic to basic rocks of Cuscatlan Formation.

In the Project Area, Morazan Formation composed mainly of basalt and agglomerate occupies the widest area (Fig.7.1). Balsamo Formation is seen in Cacahuatique Mountain. Cuscatlan Formation is scattered in small areas. The basin in the vicinity of Carolina Town is covered by quaternary deposits.

7.2 Geological Investigation

7.2.1 Past Geological Investigations

The Pre-Feasibility Study of the Torola River Basin was carried out in 1999. In the Pre-Feasibility Study, seven candidate project sites were investigated by Harza Co. Ltd. The outline of the study is as follows.

Aerial photographs were interpreted and distribution maps of lineament were made for the Torola River basin. A brief geological mapping, seismic prospecting and laboratory tests for concrete aggregate were performed for the areas of El Chaparral, Carolina and La Honda project sites. The quantity of the seismic prospecting in these projects is shown in the table below. (Table 7.1)

Table 7.1 Seismic Prospecting in Pre FS Study

Project	Seismic Prospecting
El Chaparral	6 spreads 780 m
Carolina	3 spreads 455 m
La Honda	3 spreads 405 m

Laboratory tests were conducted with the samples obtained from pits. Tested items were density, absorption, Atterberg limits, abrasion and stability.

7.2.2 Geological Investigation in Feasibility Stage

(1) Outline

The geological investigation in this feasibility stage is outlined in Table 7.2, Fig 7.2 and Fig. 7.3. This investigation was subcontracted to Swissboring Overseas Corp. Ltd, which commenced its work in October 2000 and finished it in March 2003. Field works were conducted in the dry season, and not in the rainy season (May through October), in which road conditions are poor and the crossing of the Torola River is difficult due to an increase in the river flow.

(2) Geological Mapping

The geological mapping was conducted at the El Chaparral dam site using a 1:1000 topographical map.

(3) Seismic Prospecting

During the fieldwork, Geometrics Smartseis was used for observation. The elastic wave was generated by a hammer and was observed by geophones set along the observation line at an interval of 10 m. Each spread was 130m long. The observed data was analyzed in the field by the S.I.P.Q.C program of Rimrock Geophysics. The results are shown in the velocity layer profiles.

(4) Core Boring and Permeability Test

Equipment used in core boring and permeability test are shown in Table 7.3.

Table 7.2 Quantity of Geological Investigation Work

Geological Mapping

Area	Quantity (km ²)
El Chaparral dam site	0.86

Seismic Prospecting

Area	Name of Prospecting Line	Quantity	
		(lines)	(m)
El Chaparral Dam Site	CBS-1		650
	CBS-2		260
	CBS-3		260
	CBS-4		260
	CBS-5		260
Subtotal		5	1690
Borrow Area	CGS-1		390
	CGS-2		130
	CGS-3		130
	CGS-4		130
	CGS-5		390
	CGS-6		130
	CGS-7		130
Subtotal		7	1430
TOTAL		12	3120

Core Drilling and Permeability Test

Area	Name of Drill Hole	Q'ty of Core Drilling		Q'ty of Permeability Test (section)
		(holes)	(m)	
El Chapparal Dam Site	CDB-1		70	14
	CDB-2		60	10
	CDB-3		50	6
	CDB-4		80	9
	CDB-5		70	11
	CDB-6		70	8
	CDB-7		50	8
	CDB-8		50	2
Subtotal		8	500	68
Borrow Area	CGB-1		10	
	CGB-2		10	
	CGB-3		1.7	
	CGB-4		10	
	CGB-5		10	
Subtotal		5	41.7	
TOTAL		13	541.7	68

Laboratory Tests

Excavation and Tests		Quantity	ASTM Standard
Excavation	Pit (each 3 m deep)	6 pits	
	Rock	1 place	
Concrete Aggregates Test	Samples obtained from Outcrops	1 set	C127, C131, C535, C88, D2938, C295, C289, C227
Concrete Aggregates Test	Samples obtained from River Floors	6 sets	C127, C128, C131, C535, C88, C136, C142 etc.
Intact Rock Core Test		13 sets	D2938
Petrological Analysis	Microscopic Observation	5 samples	
	X-Ray Diffraction	5 samples	

Table 7.3 Equipment of Core Boring and Permeability Test

Investigation Work	Equipment	Popular Name	Specifications
Core boring	Boring machine	Longyear 34	Drilling capacity 275m with HQ
	Pump	FMC535	Flow rate of 135 l/min at 500 psi
	Rod and core barrel		HQ and NQ
	Bit and reamer		HQ and NQ
	Casing and casing shoe		HW and NW
Permeability test	Flowmeter and pressure gage		
	Air compressor	Aerosub-plus	6000 psi compressor and 3 air bottle of 2500 psi
	Packer		HQ pneumatic packers

Core boring was conducted at the El Chaparral dam site and its borrow area. The size of a drillhole is NQ, and the diameter of the drilled core is 47.6 mm. The Lugeon test was conducted as a permeability test in drillholes at the dam site. In drillholes CDB-5 and CDB-6 on the right bank of the dam site, adequate Lugeon tests were not conducted. Therefore, reborings were made at about 5 m away from the original drillholes.

Drilled cores were arranged in wooden boxes, photographed and logged in a format showing core recovery, RQD, Lugeon value, geological description and rock classification which is based on the standards shown in Table 7.4.

Table 7.4 Standards of Rock Classification of J-Power for Drilled Core

Class	Weathering	Hardness	Crack Spacing
1	Very fresh. No weathering of mineral component.	Very hard. Broken into knife-edged pieces by strong hammer blow.	over 30 cm
2	Fresh. Some minerals are weathered slightly. Usually, no brown crack.	Hard. Broken into pieces by strong hammer blow.	10 to 30 cm
3	Fairly fresh. Some minerals are weathered. Cracks are stained and with weathered mineral.	Brittle. Broken into pieces by medium hammer blow.	5 to 10 cm
4	Weathered. Fresh portions still remain partially.	Very brittle. Easily broken into pieces by slight hammer blow.	1 to 5 cm
5	Strongly weathered. Most of minerals are weathered and altered to secondary minerals.	Soft. Able to dig with hammer.	under 1 cm

In drillholes at the dam site, the water level is monitored by CEL.

(5) Laboratory Test

Tests were conducted to identify the physical property and petrology using the drilled core obtained at the dam site. Tests were also performed for the evaluation of the quality of concrete aggregate using river deposits collected from pits in the borrow area and samples collected by the excavation of an outcrop of basalt in the vicinity of the dam site. (Table 7.5)

Table 7.5 Sample and Test Method of Laboratory Test

Location	Sample	Item	ASTM
Physical Property and Petrology	Boring core at dam site	Density	D2938
		Unconfined compression strength	D2938
		Microscopic observation	
		X-ray diffraction	
Quality of Concrete Aggregate	Basalt at the vicinity of dam site	Density	D2938
		Unconfined compression strength	D2938
		Soundness (Na ₂ SO ₄)	C88
		Abrasion	C131, C535,
		Alkali aggregate reaction	C295, C289, C227
		Dry Density	C127,
	River deposits in borrow area	Absorption	C127,
		Particle Size Distribution	C136
		Clay Lumps and Friable Particle	C142, C123
		Soundness (Na ₂ SO ₄)	C88
		Abrasion	C131, C535
		Dry Density	C127, C128
		Absorption	C127, C128

7.3 El Chaparral Project Area

7.3.1 Reservoir Area

(1) Geology

In the El Chaparral reservoir area, mountains standing close to the Torola River are not high and contain gentle slopes. This area is covered by tertiary Morazan Formation with overlying quaternary deposits (Fig.7.1). Morazan Formation is composed mainly of basalt and volcaniclastic rocks. Basalt is emplaced as lava flows and composed both of hard portions and brittle portions as observed at the dam site, and it generally provides the jointed and permeable rockmass, which forms V shaped valleys and steep slopes along the Torola River. Volcaniclastic

rocks are composed of volcanic ash, lapilli, and blocks, and generally provide compact and massive rockmass with few joints. Rocks containing few lapilli and blocks are easily weathered into soft rockmass.

(2) Water-tightness

The reservoir area occupies the lower part of the Torola river valley and is isolated from the adjacent river basin by wide mountain bodies. Tributaries flowing into the reservoir area keep their river flows in all seasons up to the elevation higher than the planned high water level of the reservoir. This indicates that the groundwater level at and around the reservoir area is high and ensures the water-tightness of the reservoir. The mountain bodies or ridges close to the dam site are not wide, but a spring and water flows on the slope of these mountain bodies or ridges were observed in the dry season (in March 2003) about 1300 m and about 700 m away from the dam site on the left bank and the right bank respectively.

(3) Slope Stability

In the reservoir and its surrounding areas, slopes are gentle in general. Topography showing landslides and thick talus deposits were not observed on the slopes, where downslopes will be washed by future reservoir water. Therefore, no slopes are likely to become unstable by the reservoir. (Fig.7.4).

(4) Others

One hot spring at the Torola River side about 2 km NNW of Carolina Town is famous in the reservoir area. It is 80 to 100 degrees in centigrade and contains Na^+ , SO_4^{2-} , HCO_3^- and SiO_2 (CEL 1996).

Active faults generally move periodically in the late Quaternary at an interval of several thousand years and topographies formed by fault actions were observed. Topographies indicating active faults were not detected in the project area through the interpretation of aerial photographs.

7.3.2 Dam Site

(1) Topography and Geology

The El Chaparral dam site is located in a narrow straight valley about 1.5 km long, and its river bed is about 30 m wide. Along this valley, terraces with gently inclined surfaces are distributed intermittently at about 180 m in elevation. Lower slopes between these terraces and river bed are steep, and cliffs are formed on some slopes. Upper slopes behind these terraces are gentle. Slopes

on the left bank climb up to the elevation higher than 250 m at the location 200 to 400 m away from the river. Those on the right bank climb up to the ridge of 200 m to 240 m in elevation at the location less than 150 m in distance. However, these ridges have some saddles and therefore, do not go higher than this level in the areas within a 400-to-600 m radius from the river. Beyond these areas, the ridges rise steadily toward the peaks higher than 300 m in elevation.

The El Chaparral dam site is located close to the downstream end of the straight valley. Its right abutment is situated in the most downstream ridge among the low ridges mentioned above. This ridge starts to rise at the second saddle located 400 m in distance from the river, and the point of the saddle is closest to the river among the three ridges. On the left bank of the dam site is a terrace where gentle surfaces incline at 5 to 20 degrees at the elevation of about 185 m. The lower slope in front of this terrace is steep at 70 degrees in average. The upper slope behind the terrace is at about 30 degrees. On the right bank, terraces are not formed, and a slope elevates itself to 220 m at 40 degrees on average.

It reaches the top of the ridge at 230 m in elevation. This ridge, with two saddles of 225 m and 220 m, does not rise in elevation up to the second saddle located about 400m in distance from the river.

Underneath the dam site are basalt, agglomerate and tuff of Morazan Formation.
(Fig 7 5, Fig.7 6 and Fig.7 7)

Basalt provides two kinds of rockmass. One is dark gray in color and hard, and its phenocrists are mainly composed of plagioclase and pyroxene. The other is reddish gray in color and somewhat brittle, and its phenocrists are mainly composed of plagioclase and biotite. (Table 7.6) On the cliff face at the dam site, bedded dark gray basalt intercalated with reddish portions were observed. Some contacts of the dark gray portions and reddish portions are gradual as observed at the riverbed and drilled core. Basalt is lava emplaced on the land and some portions became reddish and brittle when they were exposed to the atmosphere and cooled. Some portions of the basalt look like and are believed to be intermediate facies of basalt and agglomerate. This agglomeratic lava seems to exist underneath other lavas. (Table 7.6 and Fig. 7.7)

Table 7.6 Petrography of Basalt at El Chaparral Dam Site

Lithology	Drillhole	Depth		Petrography
		(m)		
		From	To	
Basalt: reddish grey	CDB-1	50.34	50.45	Andesite: Plagioclase, biotite, (chlorite)
Basalt: Dark grey	CDB-2	47.10	47.20	Basalt: Plagioclase, pyroxine, (chlorite)
	CDB-4	39.00	39.09	Basalt: Plagioclase, pyroxine, olivine

The tuff ranges from fine grained tuff to lapilli tuff, and is reddish gray, yellowish gray or greenish gray in color. The thickness of the tuff bed is generally less than 5 m. Some beds are more than 18.5m.

Thick tuff beds are stratified. Lapilli tuff beds are confirmed in drillholes of CDB-5A and 6A. They are of the same stratigraphic horizon. The lapilli tuff outcropped at the slope foot on the right bank downstream of the dam site is judged to be of the same horizon, too. The agglomeratic basalt mentioned above lies below this lapilli tuff bed.

The strata of the dam site incline roughly toward the left bank at about 10 degrees as indicated by the lapilli tuff bed. This lapilli tuff seems deformed or dislocated and does not form a continuous flat bed. This is suggested by the fact that the lapilli tuff exposed on the right bank does not continue to the left bank. It is difficult to confirm the correlation among other tuff beds through the examination of drillholes. CDB-5A and CDB-6A have other drillholes about 5m aside. In these drillholes located in very short distance, tuff beds are different in depth and thickness. These occurrences of tuff beds may have been caused by faults but are more likely to be attributed to the lack of continuity of the original tuff beds.

The surface deposits are river deposits, terrace deposits and talus deposits, and their depths are shown in Table 7.7.

River deposits are composed of round gravel and sand but their distribution is limited to the vicinity of the dam site because of the many rocks exposed on the river bed. Terrace deposits are exposed at the road cut on the left bank upstream of the dam site and consist of gravel and sand containing round gravel. In drillhole CDB-3 at the dam site, this deposit is found down to the depth of 7.75 m. Talus deposit are distributed on the foot of the slope adjacent to the river bed, and 4.8 m thick deposits are confirmed in CDB-3. They are also distributed in the vicinity of the contact of the terrace and the upper slope behind the terrace. Some valley slopes are covered by talus deposits. Talus deposits on other portions of the slopes are thin (1.25 m and 1 m thick in drillhole CDB-4 and CDB-7 respectively. Those on slopes close to the ridge are also thin as

observed at road cuts. The materials collected as soil such as drilled core in drillholes CDB-5A and CDB-6A to the depth of 7.5 m and 10.5 m respectively were judged to be residual soil or strongly weathered rock.

Table 7.7 Thickness of Surface Deposits

Name of	Location	Elevation	Length	Surface Deposits	
Drillhole		(m)	(m)	Kind of deposits	Thickness in m
CDB-1	Left bank	208.84	70.0	Talus deposit	2.05
CDB-2	Left bank	183.95	60.0	Talus and Terrace d.	7.75
CDB-3	River bed	136	50.0	Talus deposit	4.8
CDB-4	Right bank	222.45	80.0	Talus deposit	1.25
CDB-5	Right bank	225.45	70.0	Residual soil	7.5
CDB-6	Right bank	220.48	70.0	Residual soil	13.5
CDB-7	Left bank	184.06	50.0	Talus deposit	7.95
CDB-8	Right bank	204.33	50.0	Talus deposit	1

In the vicinity of the dam site, the Torola River bed runs straight for about 1.3 km to the direction of N 30 W, which was interpreted as a lineament suggesting a fault zone in the Pre-FS study. The fact that the lapilli tuff exposed on the right bank does not continue to the left bank, as well as the existence of small fault planes with striation observed at the river bed also point to the possibility of a lineament. Some lineaments composed of a liner distribution of saddles and small valleys that were also revealed in the Pre-FS report may indicate the existence of faults. However, the fault zone along the river bed is narrow because the exposed rocks at the river bed are not sheared strongly.

The dark gray basalt is jointed. Platy joints have been developed in some locations. However, the joint system with distinguished orientation was not observed in particular.

At the dam site, hard and fresh rocks are exposed at the river bed, while rocks are strongly weathered on the upper slope and ridge. The thickness of the strongly weathered layer is shown in Table 7.8.

Table 7.8 Thickness of Highly Weathered Layer in Drillhole

Name of Drillhole	Location	Elevation (m)	Length (m)	Highly Weathered Layer thickness (m)	depth of bottom (m)
CDB-1	Left bank	208.84	70.0	0	2.05
CDB-2	Left bank	183.95	60.0	0	7.75
CDB-3	River bed	136	50.0	0	4.8
CDB-4	Right bank	222.45	80.0	8.05	9.3
CDB-5	Right bank	225.45	70.0	4.5	12
CDB-6	Right bank	220.48	70.0	17.5	32
CDB-7	Left bank	184.06	50.0	0	7.95
CDB-8	Right bank	204.33	50.0	2.7	3.7

The strongly weathered layer is distributed very little at the river bed and on the left bank, while it becomes 10m or more in thickness on the right bank. In the CDB-6 hole, the strongly weathered layer is 17.5 m thick. The total thickness of this layer and the residual soil is 32 m. The thicker layer is attributable to the tuff, which is weathered more easily than basalt.

(2) Geotechnical Study

Boring cores obtained at the dam site is classified based on the standards shown earlier in Table 7.4. In these standards, drilled cores were classified in terms of weathering, hardness and crack spacing.

The fresh rocks at the dam site are abbreviated as follows.

Dark gray basalt	(BD)	Hard but jointed
Reddish gray basalt	(BR)	Somewhat brittle and jointed
Agglomeratic basalt	(BAg)	Somewhat brittle and not so jointed
Tuff	(Tf)	Brittle and not so jointed

The unconfined compressional strength of these rocks is compared in Fig. 7.8. The strength of the rocks of dark gray basalt ranged from 800 to 1200 kgf/cm², while the strength of the reddish the gray basalt, the agglomeratic basalt was about 200, kgf/cm². The strength of the tuff was about 100 kgf/cm².

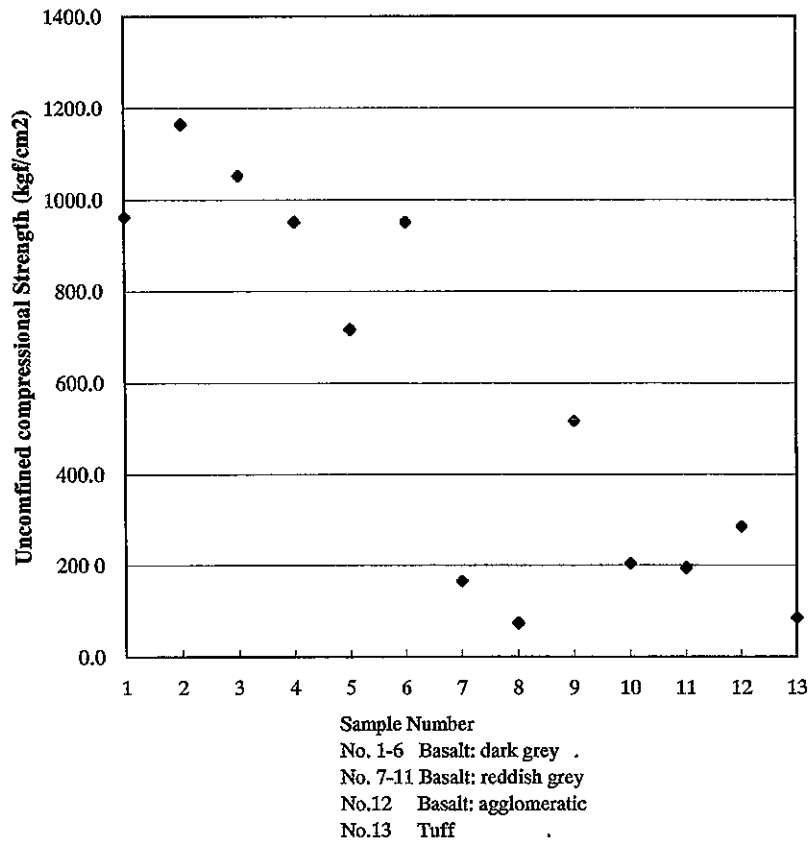
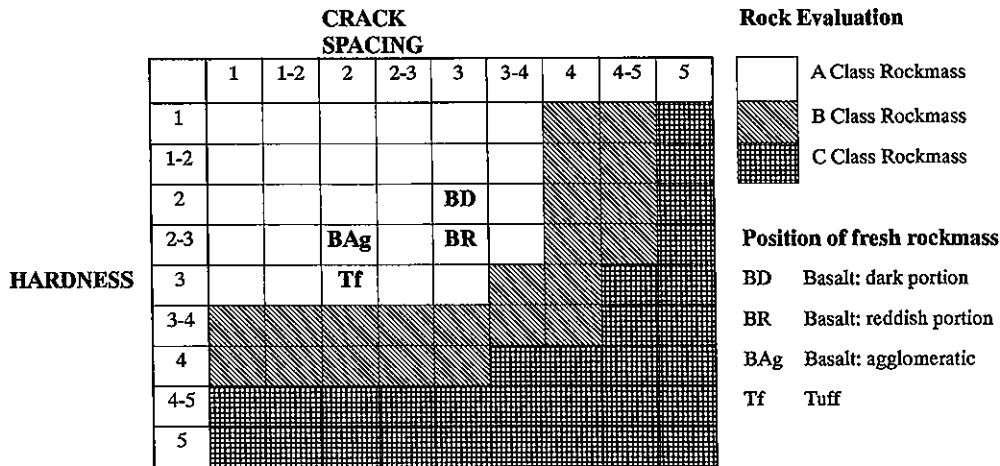


Fig.7.8 Unconfined Compression Strength

The rockmass was categorized into A, B and C classes, based on the combination of hardness and crack spacing, as shown in Table 7.9.

The Class A rockmass does not pose any problem as the basement rock of a concrete gravity dam. This class corresponds to the Japanese class that is judged suitable for the basement rock of concrete gravity dams. Class B would require careful investigation and study. Class C denotes to a strongly weathered rock, and it should be removed from the foundation of dams. This evaluation should be revised for improved reliability by performing detailed investigations during the Definite Design stage. In Table 7.9, the position of fresh rocks at the dam site is also shown.

Table 7.9 Rockmass Evaluation



This evaluation is shown in log of drillholes on profiles of the dam site. (Fig.7.6 and Fig.7.7). The depth to the surface of A class rockmass is shallow on the left bank and deep on the right bank. The depth to the surface of B class rockmass is deeper on the right bank, too. (Table 7.10)

Table 7.10 Thickness of B and C Class Rockmass

Name of Drillhole	Location	Elevation (m)	Length (m)	C class Rockmass		B class Rockmass		Total thickness (m)
				thickness (m)	depth of bottom (m)	thickness (m)	depth of bottom (m)	
				CDB-1	Left bank	208.84	70.0	
CDB-2	Left bank	183.95	60.0	0	7.75	0	7.75	0
CDB-3	River bed	136	50.0	0	4.8	0	4.8	0
CDB-4	Right bank	222.45	80.0	8.05	9.3	11.2	21	20.5
CDB-5	Right bank	225.45	70.0	4.5	12	2.8	14.8	7.3
CDB-6	Right bank	220.48	70.0	20.5	31	1	32	21.5
CDB-7	Left bank	184.06	50.0	0	7.95	2.05	10	2.05
CDB-8	Right bank	204.33	50.0	2.7	3.7	4	7.7	6.7

As described before, the fault along the river bed is not accompanied by a wide sheared zone.

Tuff beds have the least strength among the rocks at the dam site. They get softer by weathering. Only tuff beds that dip gently and are continuous and smooth in profile may be too weak to serve as sturdy layers to ensure the stability of the foundation rock of the dam. The tuff beds at the dam site are not continuous with a significant relief. Therefore, they should not affect the stability of foundation rock of the dam site.

(3) Hydrogeology

The groundwater level at the dam site was measured in drillholes. Fluctuations in the water levels as measured in drillholes were recorded for about two years on the left bank, and for about one year on the right bank (Fig.7.9). The water level in drillholes rose in the rainy season and drops in the dry season. The rise in the water level during the rainy season was small and limited to 5 m

or less for CDB-4, CDB-5 and CDB-8; whereas an increase of more than 30m was reported for CDB-1 and CDB-6.

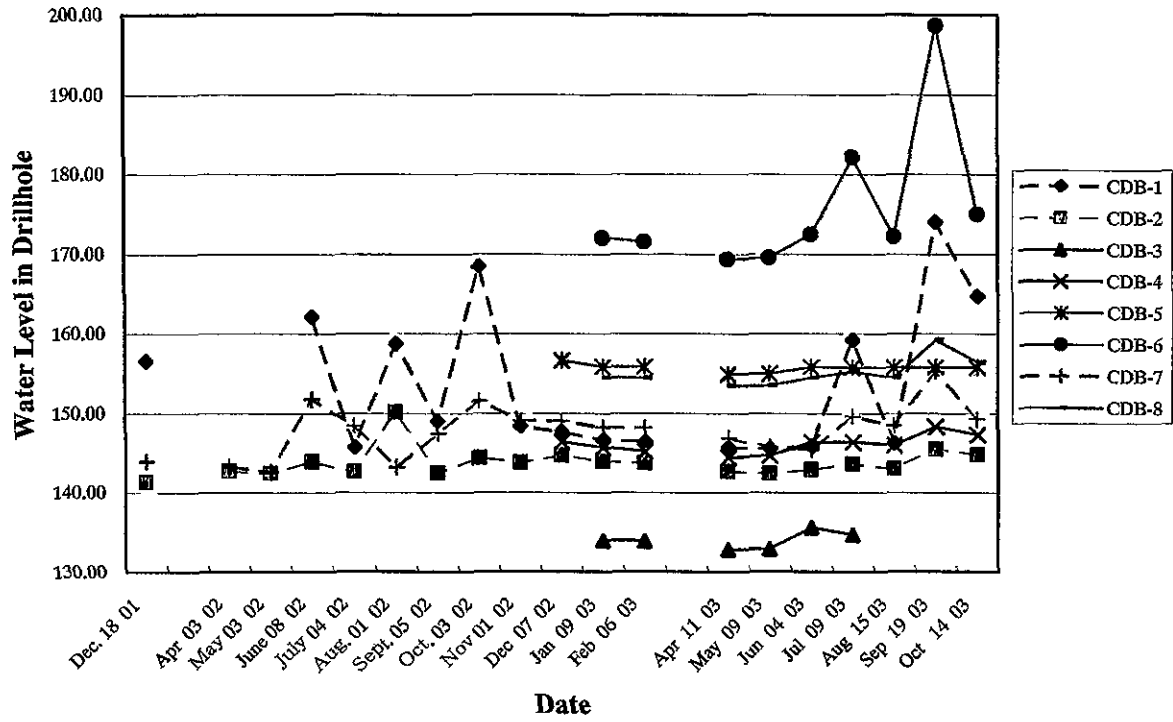


Fig. 7.9 Water Level in Drillhole

The water level on February 6, 2003 is presented in the geological profiles of the dam site (Fig 7.6 and Fig. 7.7) and the contour of groundwater table (Fig.7.10).

The groundwater level at this dam site is low; in other words, the difference in the water level between the dam site and at the drillholes farther away from the river is small. On the left bank, a difference in the ground water level of about 10 was observed between drillhole CDB-2 and the river site, and about 15 m between drillhole CDB-7 and the river side. Both holes are about 60 m away from the river. The difference in the ground water level was about 13 m for drillhole CDB-1, which is situated about 150 m from the river. At the location about 1300 m south of the dam site and about 700 m away from the river, one spring and a water flow named San Antonio tributary were observed during the dry season (March 2003) in the areas higher than 300 m in elevation, which indicates the ground water level in their vicinity.

On the right bank, such differences stood at 12 m and 21 m for drillholes of CDB-4 and CDB8 respectively which are located about 100m away from the river. The difference of 22 m was confirmed for CDB-5 about 270 m away from the river and about 32 m for the CDB- 6 hole about 400m distant from the river. In a small tributary on the right bank, water flows during the dry

season (in March 2003) at the elevation of about 220 (about the same as the planned high water level) about 600 m away from the river. This water flow indicates a rather high groundwater level in the vicinity.

(4) Permeability

Permeability tests were conducted in the drillholes at the dam site. Lugeon values for drill holes are presented in geological profiles of the dam site. (Fig.7.11). Many of the tested sections (61% of all sections) had more than 10 Lu. 35% of the sections tested on the right bank had more than 20 Lu.

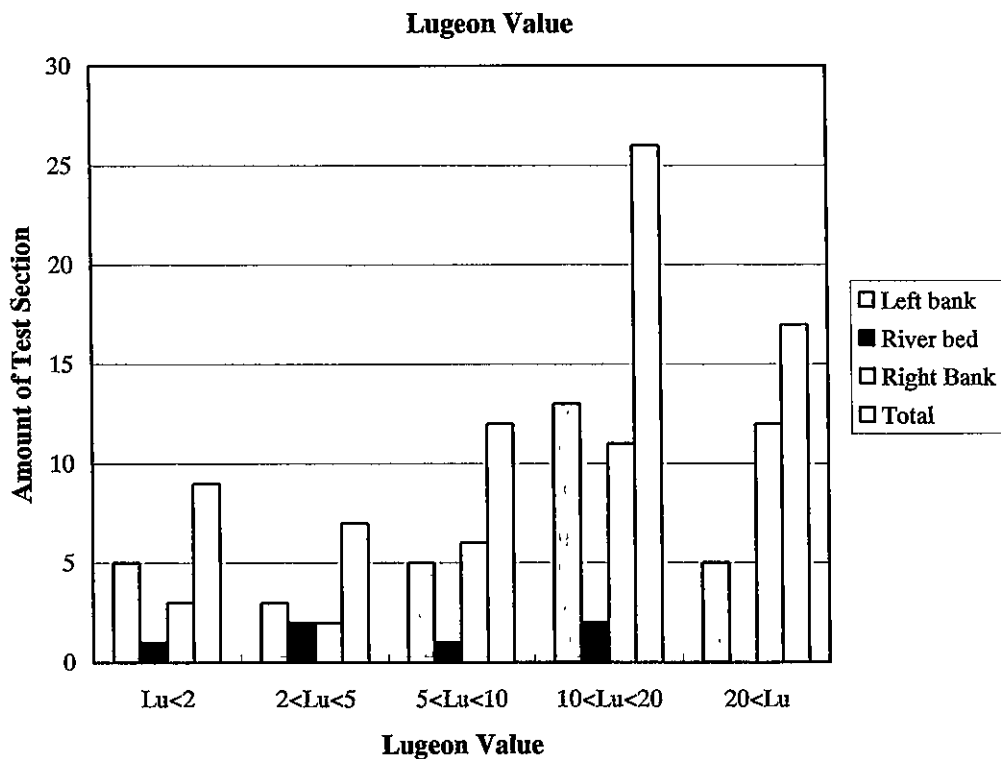


Fig.7.11 Distribution of Lugeon Values at Dam Site

Most of the tested sections in drillhole CDB-5A showed values of more than 20 Lu. This hole is the most permeable hole at the dam site. In drillhole CDB-5A, many tested sections show a critical pressure. Lugeon values obtained at the effective injection pressure of less than 6 kg/cm² or 7 kg/cm² were less than 10, whereas, in the same section, the Lugeon values increased significantly to more than 20 at a pressure level higher than these pressures. The critical pressure is between 6 kg/cm² or 7 kg/cm² and the higher pressure adopted in the next pressure stage. The Lugeon values before reaching the critical pressure were adopted in this study. The validity of the use of these values is supported by the fact that the pressure at the high water level acting to the

CDB-6A hole is lower than the critical pressure and that the water level of the CDB-6A drillhole remains relatively high.

At the CDB-3 hole at the river bottom, three out of the six sections showed less than 5 Lu. Deep portions of both abutments were out of reach by drillholes but they are low in permeability given the result of the CDB-3 hole.

The results of permeability tests do not show any distinct hydrogeological difference among different lithology. The dark gray basalt is presumably most permeable but the actual difference was not clear from the test results. Some small springs are observed in the vicinity of the river bed on the right bank at the dam site during the dry season. These springs scatter in a section about 200 m long along the river. Their individual discharge seems to be about 10 l/sec. This group of small springs indicates the existence of a connected network of joints which make the rockmass permeable.

The permeability of the agglomeratic basalt is likely to be low, as suggested by many test sections having Lugeon values of less than 10. However, this tendency has not been confirmed.

The tuff beds appear to be able to act as barriers, because a small spring was observed at the contact of the tuff and the overlying agglomerate on the right bank about 1km downstream from the dam site. However, tuff beds do not act as barriers, because the water level during the drilling did not change significantly when the tuff beds were penetrated by drilling. The hydrogeological behavior of the tuff bed indicates its lack of lateral continuity or a development of joints in tuff beds.

Thus, at the dam site, any significant hydrogeological structure controlled by geology was not confirmed. The rockmass at the dam site is generally permeable and decreases in permeability as the depth increases.

7.3.3 Power Station

The power station site is planned on the left bank about 120 m downstream of the dam site. In order to keep an open space for the power station, the slope at the power station site will be excavated. This slope climbs up to about 180 m in elevation at 50 degrees. Above the elevation of 180m, the slope is gentle at about 15 degrees.

One core boring (CDB-7, 50 m long) was conducted in the vicinity of the power station site. A seismic prospecting (CBS- 2) was also conducted.

The gentle slope above El 180 m is covered with talus deposits, which is 7.95 m thick in drillhole CDB-7. Below this talus deposits, hard basalt is confirmed at the depth from 11 to 50 m (the bottom of the drillhole and close to the elevation of the river bed) in CDB-7. (Fig.7.12)

The foundation rock of the power station, for which a deep excavation will be planned, is hard basalt and is considered stable enough.

The stability of cut slopes is important at the power station site. In drillhole CDB-7, basalt is composed of dark gray portions and reddish gray portions and the former is dominant. No tuff bed was encountered there. Because basalt lava inclines toward the left bank, the contacts of each lava flow do not decrease the stability of cut slopes. The steep slope continuing from the dam site to the power station site at 50 to 70 degrees are free of discontinuities that may affect slope stability and guarantees the stability of the cut slope. Therefore, the stability of the cut slope can be ensured with the countermeasures to stabilize the loosened zone close to the surface of the cut slope.

7.3.4 Construction Material

(1) Required Volume of Concrete Aggregate

For the aggregate for concrete, river bed gravel at the construction site, deposits on the terrace, and excavated materials from dam and powerhouse will be diverted. The total concrete quantity is approximately 430,000 m³; approximately 390,000 m³ for the dam body (including the upstream cofferdam) and approximately 40,000 m³ for the other structures. The rude materials required for the concrete quantity is approximately 520,000 m³, which is broken down into approximately 380,000 m³ of rough aggregate and approximately 140,000 m³ of fine aggregate.

(2) Quality of Concrete aggregate

The items for the evaluation of the quality of concrete aggregate based on ASTM C33-2001 and JIS as a point of reference are shown in Table 7.11.

Table 7.11 Requirement for Quality of Concrete Aggregate

Standard of ASTM C33-2001

Item	Fine Aggregate	Coarse Aggregate	ASTM
Particle Size Distribution	in the requirement	in the requirement	C136
Clay Lumps and Friable Particle	≤ 3%	≤ 5%	C142, C123
Organic Impurity	Color of the liquid is thinner than the reference color solution	Not specified	C40
Material Finer than 75μm Sieve	≤ 3%(or5%)	≤ 1.0	C117
Coal and Lignite	≤ 0.5%(or1%)	≤ 0.5%	C123
Soundness(Na ₂ SO ₄)	≤ 10%	Not specified	C88
Abrasion	Not specified	≤ 50%	C131,C535
Alkali Aggregate Reaction			C295, C289, C227
Standard of JIS A5308	(for reference)		
Dry Density	≥ 2.5g/cm ³	≥ 2.5g/cm ³	C127, C128
Absorption	≤ 3.5%	≤ 3.0%	C127, C128

These items were divided into 2 groups. One group consists of items (characteristics) that can be adjusted in the process of making aggregates. The other group is composed of items (characteristics) inherent in materials such as the texture and the mineral composition of the materials, which cannot be adjusted in the process.

(3) Investigation

For the source of concrete aggregate, the river deposits of the Torola River and the basalt rock body was studied.

The investigation of river deposits was conducted at the river bed about 2 km upstream of the dam site. This site is located in a wide valley. The materials for the concrete aggregate were collected from the gravel bar which stretches about 900 m long along the river and about 100 m in width. The river bed is about 150 m wide. In the dry season, about 100 m is exposed as gravel bar, which is divided into the upstream area and the downstream area located on the right bank and the left bank respectively. The difference between the surface of the bar and the river level is 3 m at the most. The surface of the bar has many round-shaped gravels with diameters of 20 cm to 50 cm. They are mainly composed of basalt. In the vicinity of both upstream and downstream areas, basalt outcrops were observed. They suggest that the thickness of river deposits is small. Adjacent to the river bed is a terrace which is about 5m above the river level and more than 100m wide. It is covered with sand and gravel.

Seismic prospecting and core boring were conducted in order to understand the volume of river deposits. In order to examine the quality for concrete aggregates, laboratory tests were conducted with samples collected by pit excavation. (Table 7.12 and Fig. 7 3)

Table 7.12 Investigation Work in Borrow Area

Investigation	Name	Quantity	Length(m)	Remarks
Seismic Prospecting	CGS-1		390	
	CGS-2		130	
	CGS-3		130	
	CGS-4		130	
	CGS-5		390	
	CGS-6		130	
	CGS-7		130	
		7 lines		1430
Core Boring	CGB-1		10	
	CGB-2		10	
	CGB-3		1.7	
	CGB-4		10	
	CGB-5		10	
		5 holes		41.7
Pit		6 pits	18m	Each 3m in depth
Laboratory Test		6 sets		C127, C128, C131, C535, C88, C136, C142 etc.

(4) Results of Investigation

The volume of river deposits was projected by seismic prospecting. Then it was adjusted by the thickness confirmed by core boring.

The area of the bar is 90,000 m², composed of an upstream area of 100 m wide and 500 m long and a downstream area of 100 m wide and 400 m long.

The seismic prospecting helps project the thickness as profiles of the velocity layer, which is useful for the estimation of the volume for the entire area. The average thickness of all seismic prospecting lines was 4 m (Appendix 7.12.2). The assumed volume by seismic prospecting was 360,000 m³.

The thickness of river deposits confirmed by drillholes and pits and the results assumed by the seismic prospecting conducted in the vicinity of drillholes and pits are presented in Table 7.13.

Table 7.13 Thickness of River Deposit in Drillholes, Pits and Seismic Prospecting Lines

Boring & Pit	Thickness of River Deposits (m)	Reprezentative Thickness (m)	Seismic Prospecting Line	Thickness of Upper Verocity Layer (m)	Reprezentative Thickness (m)
CGB-1	6	6	CGS-1	4.5	5
CGP-1	>3		CGS-2	5.5	
CGB-2	2.7	3	CGS-1	3.5	3.75
CGP-2	>3		CGS-3	4	
CGP-6	>3.5				
CGB-3	1.7	1.7	CGS-1	4.5	3.35
CGP-3	1.5-1.9		CGS-4	2.2	
CGB-4	6.5	6.5	CGS-5	5	3.5
CGP-4	>3.25		CGS-6	2	
CGB-5	1	2	CGS-5	5	5.75
CGP-5	>2.2 or 2.7		CGS-7	6.5	
Average		3.84			4.27

The thickness confirmed by drillholes and pits is different from that indicated by seismic prospecting at some places (CGB-5). The latter is larger than the former. The average depth in drillholes and pits was 3.8 m. The average depth assumed by seismic prospecting in the vicinity of the drillholes and pits was 4.3 m.

The volume adjusted by the thickness by drillholes is:

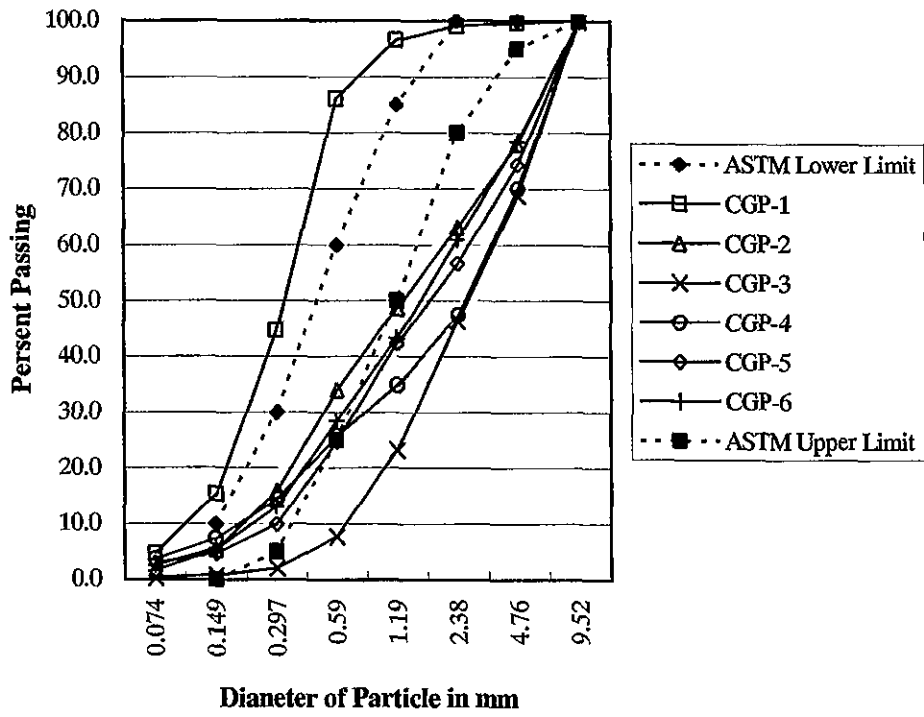
$$360.000 \text{ m}^3 \times (3.8 \text{ m} / 4.3 \text{ m}) = 318.000 \text{ m}^3$$

The quality for the concrete aggregate was studied as follows

The results of laboratory tests are shown in Table 7.14

The graph of particle size distribution is shown in Fig.7.13. In the fine aggregate, coarse particles were less than the ASTM requirement. However, it will be possible to adjust particle size distribution to meet the requirement by crushing or blending. In the coarse aggregate, fine particles exceeded the requirement. The bar provides big gravels more than and to provide the sufficient amount of coarse aggregate with the maximum dimension of 3 inches or 2.5 inches.

Fine Particle Size Distribution



Coarse Particle Size Distribution

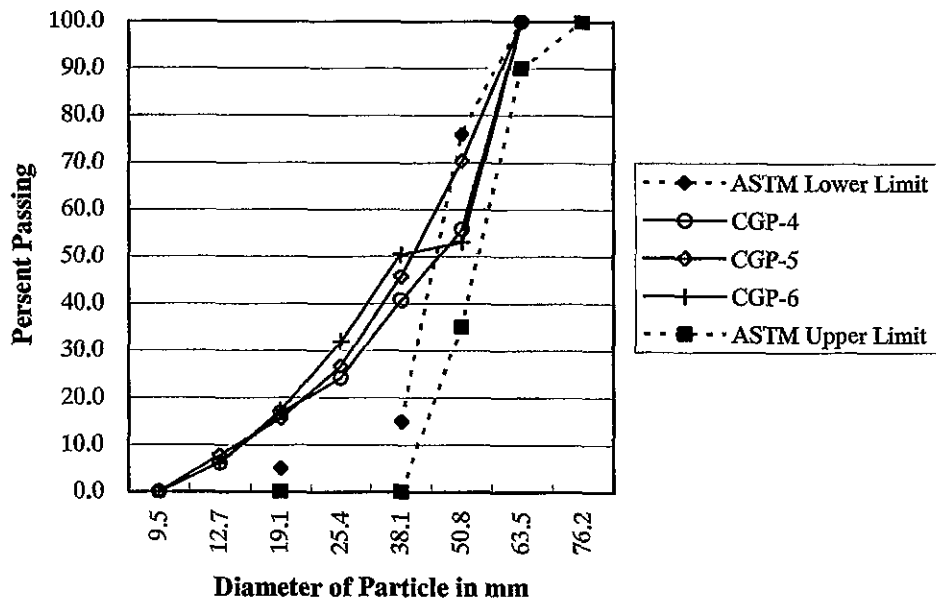


Fig.7.13 Particle Size Distribution

On organic impurity, a test was not conducted, because few humin or plant particles were observed in pits.

The test for coal and lignite was judged unnecessary, because coal and lignite particles were not observed and were not provided to the river bed from the catchment area with underlying volcanic rocks.

On abrasion, samples met the requirement.

On stability (Na_2SO_4), some samples did not meet the requirement. As described in the paragraph of density and absorption, however, this shortcoming is permitted to some extent.

On alkali-aggregate reaction, no test was conducted. Sand and gravel are composed of particles of volcanic rocks that generally show alkali-aggregate reactivity. It will be more practical to add fly ash to prevent alkali-aggregate reaction. On density and absorption, fine aggregate does not meet the JIS requirement. Samples were not evaluated to be sound. The same was also suggested by the test results of some samples which lost more than 10% when tested for stability. Some samples for coarse aggregate do not meet JIS requirement. Although they meet the requirement for abrasion, they were not evaluated to be sound enough. However, as the climate of the project area is mild and free of problems cause by freezing, the shortcoming in the texture of the aggregate is permitted to some extent.

Some results of the laboratory tests do not meet the requirements for concrete aggregate. However, materials of the bar can be utilized for concrete aggregate. This conclusion is supported by the fact that the concrete of 15 de Septiembre is not damaged. 15 de Septiembre is in the downstream of the Chaparral dam site, where concrete aggregate was made of the river deposits similar to those the investigation area.

Table 7.14 Result of Test of River Deposits

Standard of ASTM					
Item	Fine Aggregate	Result	Coarse Aggregate	Result	ASTM
Particle Size Distribution	in the requirement		in the requirement		C136
Clay Lumps and Friable Particle	$\leq 3\%$	0.5-3.4	$\leq 5\%$	No Test	C142, 123
Organic Impurity	Color of the liquid is thinner than the reference color solution	No Test	Not specified	No Test	C40
Material finer than 75 μm Sieve	$\leq 3\%$ (or 5%)	No Test	≤ 1.0	No Test	C117
Coal and Lignite	$\leq 0.5\%$ (or 1%)	No Test	$\leq 0.5\%$	No Test	C123
Soundness (Na_2SO_4)	$\leq 10\%$	4.6-22.5	Not specified	4.5-9.8	C88

Item	Fine Aggregate	Result	Coarse Aggregate	Result	ASTM
Abrasion	Not specified	No Test	≤50%	14.2-21.9	C131, 535
Alkali Aggregate Reaction		No Test		No Test	C295, C289, C227
Standard of JIS (for reference)					
Dry Density	≥2.5g/cm ³	2.3-2.43	≥2.5g/cm ³	2.26-2.75	C127, C128
Absorption	≤3.5%	3.9-6.1	≤3.0%	0.9-4.7	C127, C128

On the basalt rock body, one set of laboratory tests was conducted using a sample obtained from the outcrop on the right bank upstream of the dam site. The sample is composed of somewhat weathered basalt. The test results are shown in Table 7.15. No further investigation for basalt quarry was conducted, because a large amount of raw materials for concrete aggregate will be obtained from river deposits and also from the muck of fresh basalt supplied by the excavation of the dam and the power house.

Table 7.15 Results of Test of Basalt

Item	Fine Aggregate	Result	Coarse Aggregate	Result	ASTM
Soundness(Na ₂ SO ₄)	≤10%	No Test	Not specified	64.23%	C88
Abrasion	Not specified	No Test	≤50%	18.2%	C131, 535
Alkali aggregate reaction		No Test		(one sample only)	C295, C289, C227
Dry Density	≥2.5g/cm ³	No Test	≥2.5g/cm ³	2.56 g/cm ³	C127
Absorption	≤3.5%	No Test	≤3.0%	3.6%	C127

7.4 La Honda Project

The dam sites of the La Honda project are located about 15 km upstream of the El Chaparral dam site. The planned high water level of this project is 275 m in elevation. In the vicinity of the dam sites, The Torola River meanders in a narrow valley, and the river bed is about 220 m in elevation and about 50m wide. One bank of the valley is an undercut slope and steep, but the opposite bank is a slip-off slope which is gentle. No V-shaped valley deeper than 100 m exists. Terraces 20 m to 40 m above the river bed are formed on the slip-off slope.

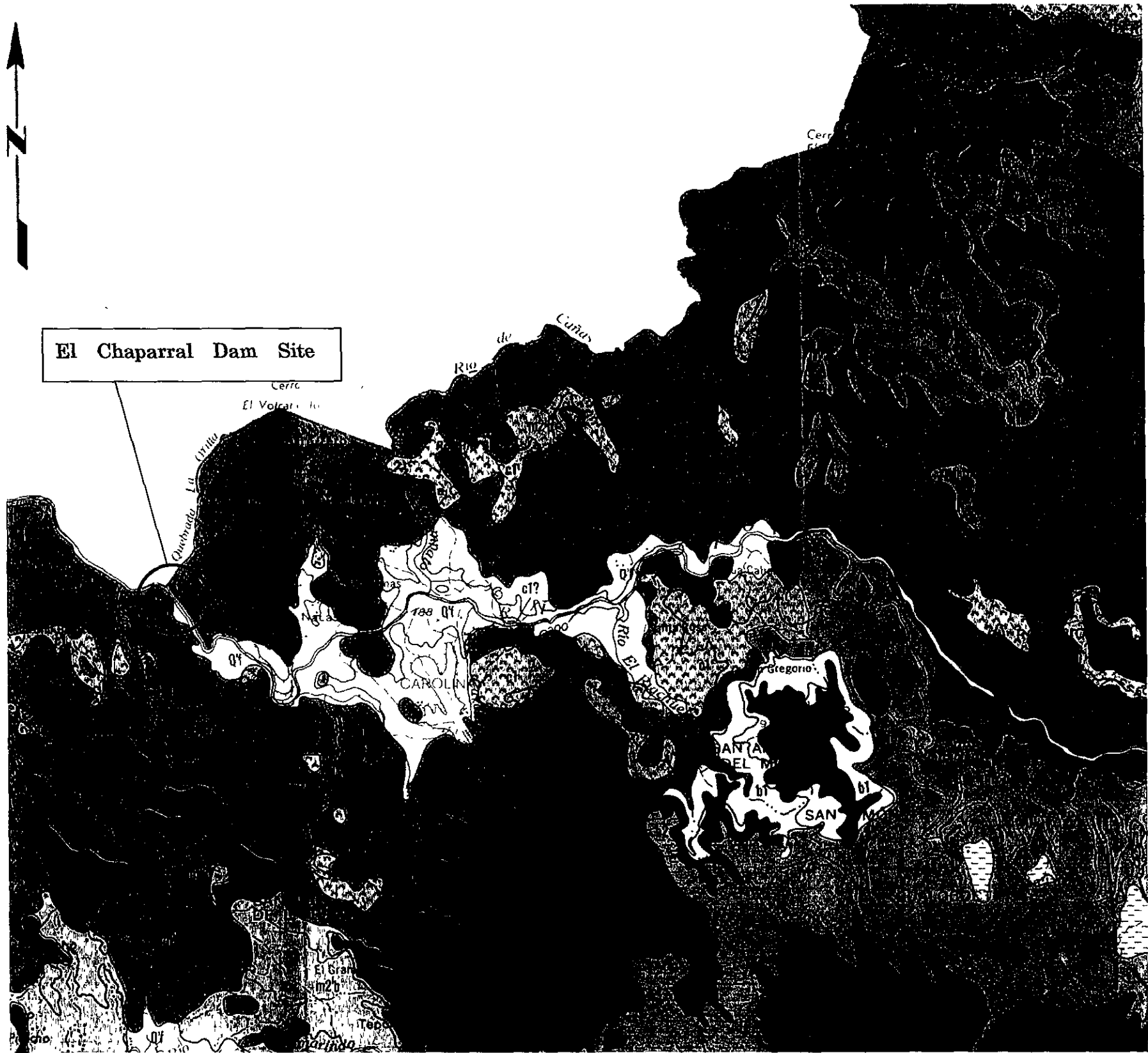
Basalt, agglomerate and tuff of Morazan Formation underlie the dam sites and its vicinity. The basalt is hard and jointed. The agglomerate is massive and rather brittle and gradually changes to basalt. Their distribution is not simple. Tuff composes the upper slope on the left bank and is massive. The strata of rocks incline gently toward the left bank. Bars composed of gravel and sand distribute intermittently on the river bed. Terraces are covered with terrace gravel, and the gentle slopes behind terraces are covered with rather deep talus deposits.

Two dam sites were briefly investigated by reconnaissance. One is the dam site adopted in the Pre-FS study, where seismic prospecting of 405 m in total length was conducted during the Pre-FS stage. The other is the upstream site.

At the Pre-FS site, the right bank is an undercut slope and steep, while the left bank shows a gentle slip off the slope. The slope 30 m to 60 m above the river bed on the left bank is gentle. This dam site has underlying basalt and agglomerate. The rocks exposed at the river bed indicate thin river deposits. A thick layer of 650 to 800 m/sec is indicated by seismic prospecting at the lower slope on the left bank. Rather thick (probably up to 10 m thick) terrace deposits and talus deposits underlie the gentle slope 30 to 60 m above the river bed. The outcrops in the vicinity of the dam site suggest that weathering is generally thin. At the dam site, the groundwater level is presumably low, because of the distribution of basalt.

The Upstream site is about 1.5 m upstream of the Pre-FS dam site. This site offers advantages in terms of topography. The slope on the right bank is very steep with few surface deposits. The slope on the left bank is also steep with one exception of a narrow gentle slope about 60 m above the river bed. The bed rock is composed of basalt. Fresh rocks are exposed in a wide area on the slope on the right bank. Many outcrops on the left bank are indicative of thin talus deposits on the slope of the left bank. The reddish tuff intercalated in basalt layers inclines southwest (toward downstream) at about 20 degrees. This dam site needs a dike at the saddle about 280 m in elevation on the left bank. This dike site shows underlying basalt and tuff, which are covered by few surface deposits. An outcrop of weathered tuff was observed. The groundwater level both of the dam site and dike site is presumably low because of the distribution of basalt.

As for construction materials, sand and gravel composing bars on the river bed are suitable for concrete aggregates, while basalt, which generally includes brittle reddish portions, will require careful operation, as in the case with the El Chaparral project. Talus deposits covering the terrace both upstream and downstream of the dam sites may be candidates for impervious core materials.

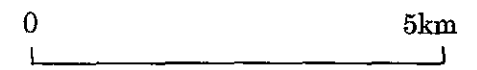


A part of 1:100,000 Mapa Geologico de la Republica de El Salvador (1978)

Cacahuatique Mountain \triangle

LEGEND

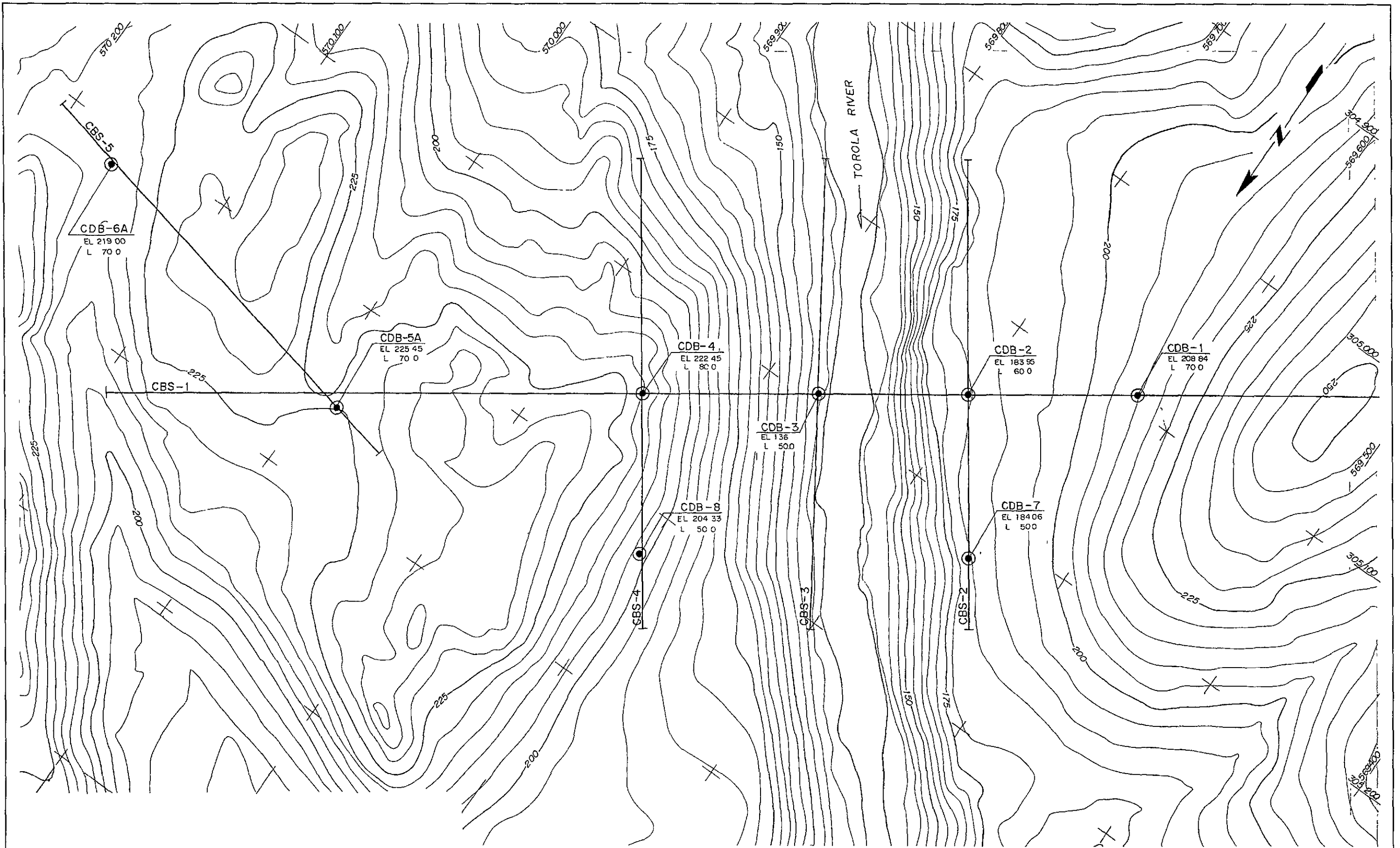
Terciario Tertiar	Pleistoceno Pleistozan	Formación CUSCATLÁN Folge	sl
		Formación BALSAMO Folge	bl
	Plioceno Pliozan	Formación CHALATENANGO Folge	
		Formación MORAZAN Folge	
	Mioceno Miozan		
	Oligoceno Oligozan		
	Eoceno Eozan		
Paleoceno Paleozan			



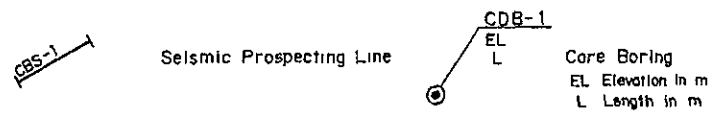
EL CHAPARRAL HYDROPOWER PROJECT

GEOLOGICAL MAP OF PROJECT AREA

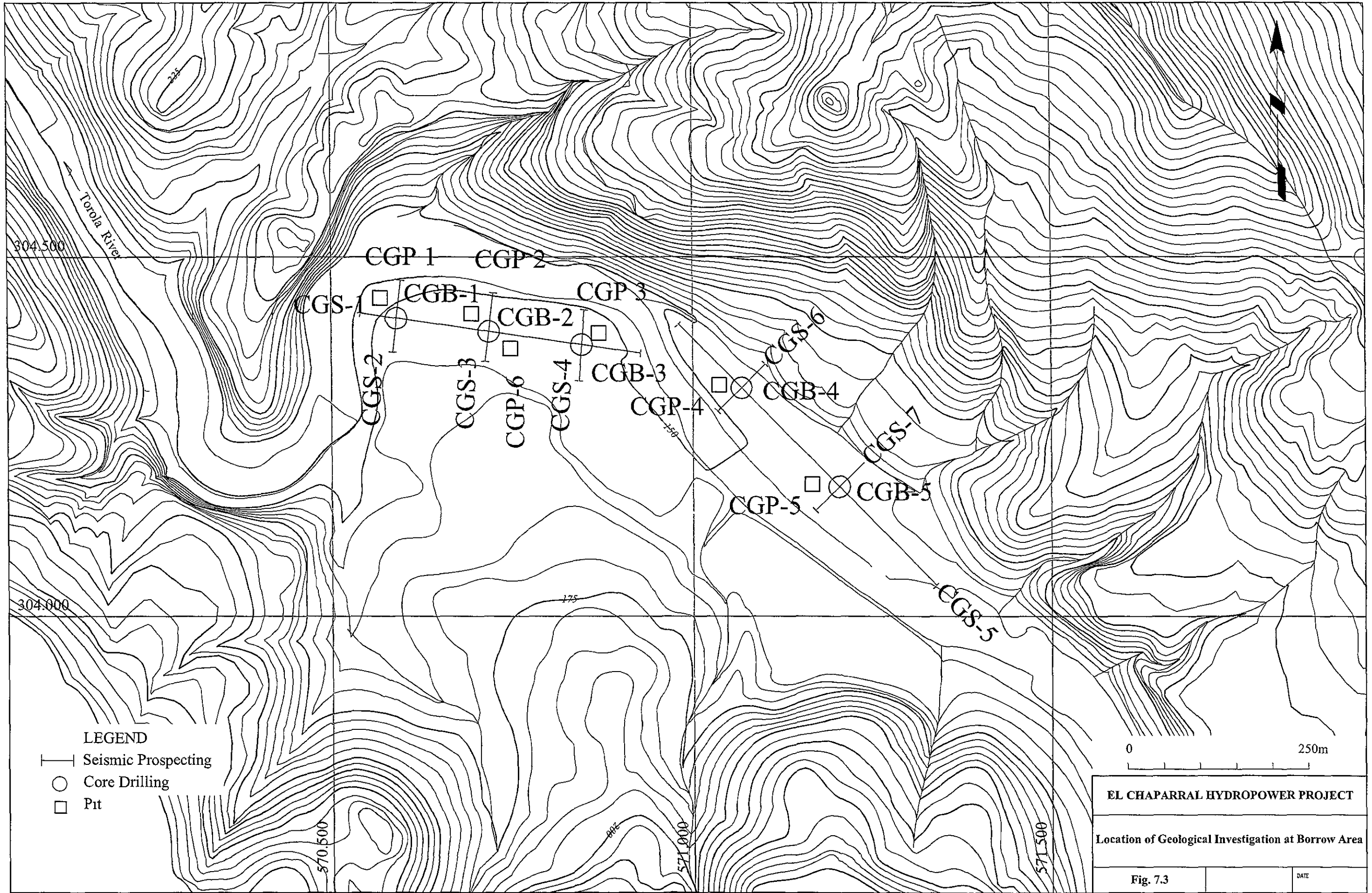
Fig 7.1 | DATE



LEGEND







EL CHAPARRAL HYDROPOWER PROJECT		
LOCATION OF GEOLOGICAL INVESTIGATION AT DAM SITE		
Fig. 7.2	DATE	



309
308
307
306
305
304
303

HONDURAS

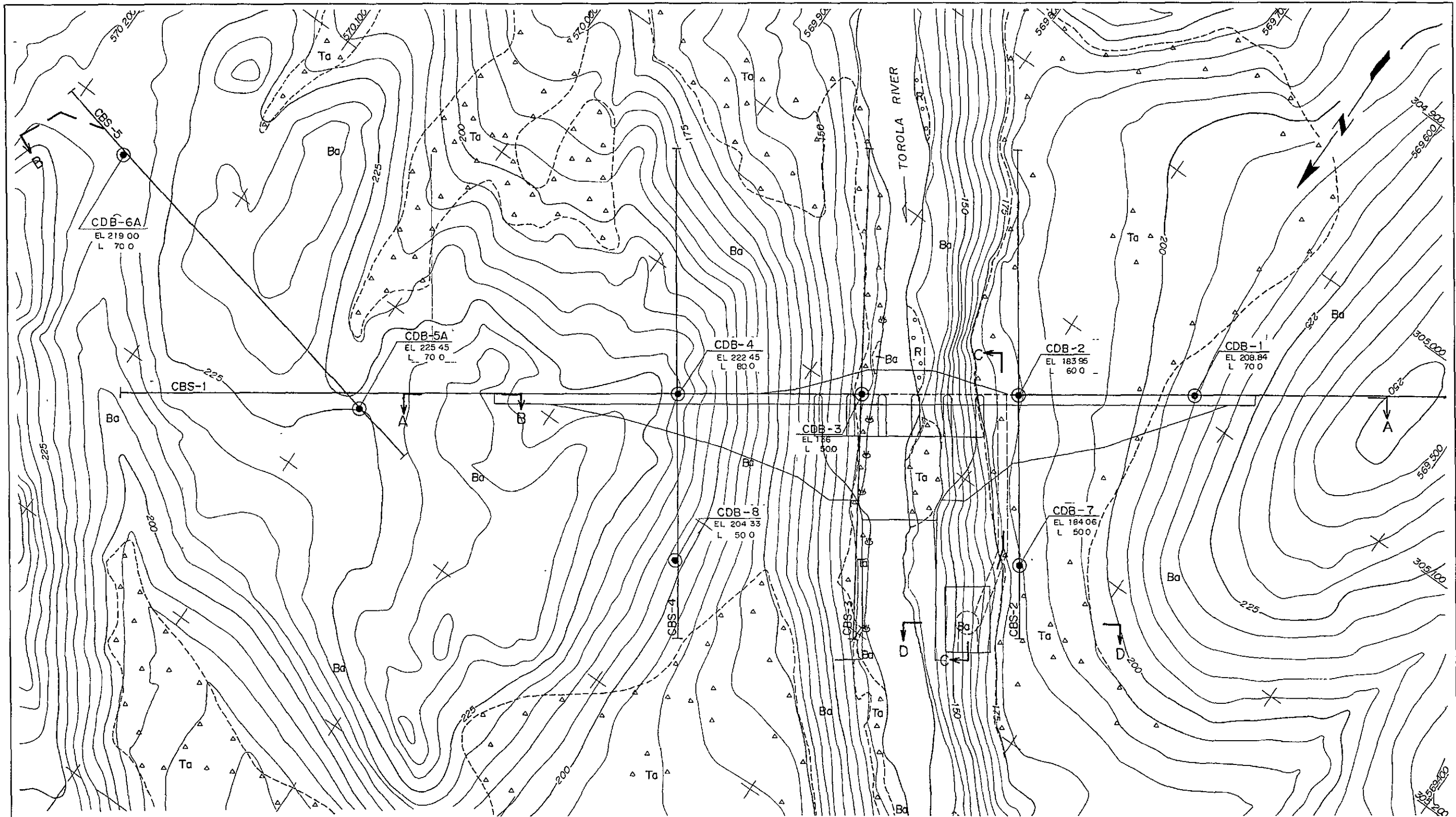
568 569 570 571 572 573 574 575 576 577 578 579 580 581

- LEGEND
-  Convex break of slope
 -  Concave break of slope
 -  Ridge or queta
 -  Assumed landslide area

0 2km

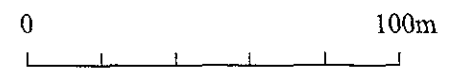
EL CHAPARRAL HYDROPOWER PROJECT		
Topographical Interpretation Map of Reservoir Area		
Fig. 7.4		DATE

2014



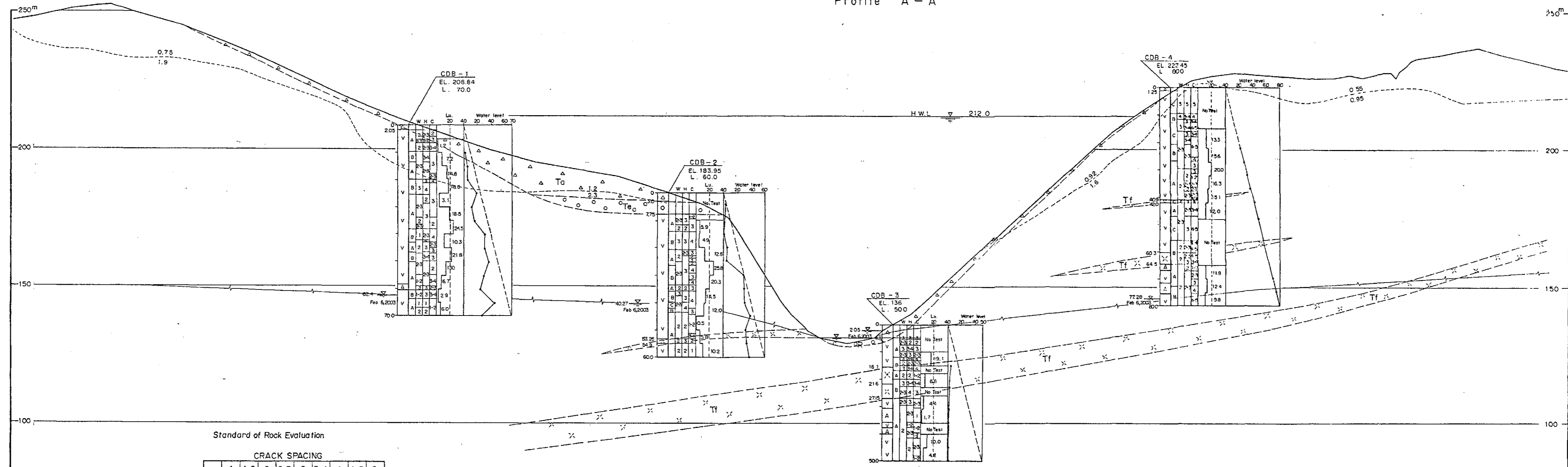
LEGEND

- △ Ta △ Talus deposit and residual soil
- R ○ Recent river deposit
- Ba Basalt
- Geologic boundary
- CBS-1
- Seismic Prospecting Line
- CDB-1
- Core Boring
EL Elevation in m
L Length in m
- Spring
- Location of Profile



EL CHAPARRAL HYDROPOWER PROJECT	
GEOLOGICAL PLAN OF DAM SITE	
Fig. 7.5	DATE

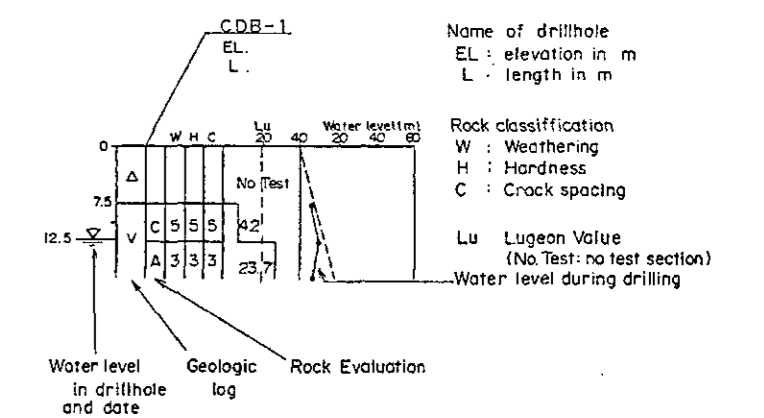
Profile A - A



LEGEND

- Talus deposits and residual soil
- Recent river deposit
- Terrace deposit
- Basalt
- Tuff
- Geologic boundary
- Ground water table
- Velocity layers and their velocity (km/sec)

(Log of Drillhole)



Standard of Rock Evaluation

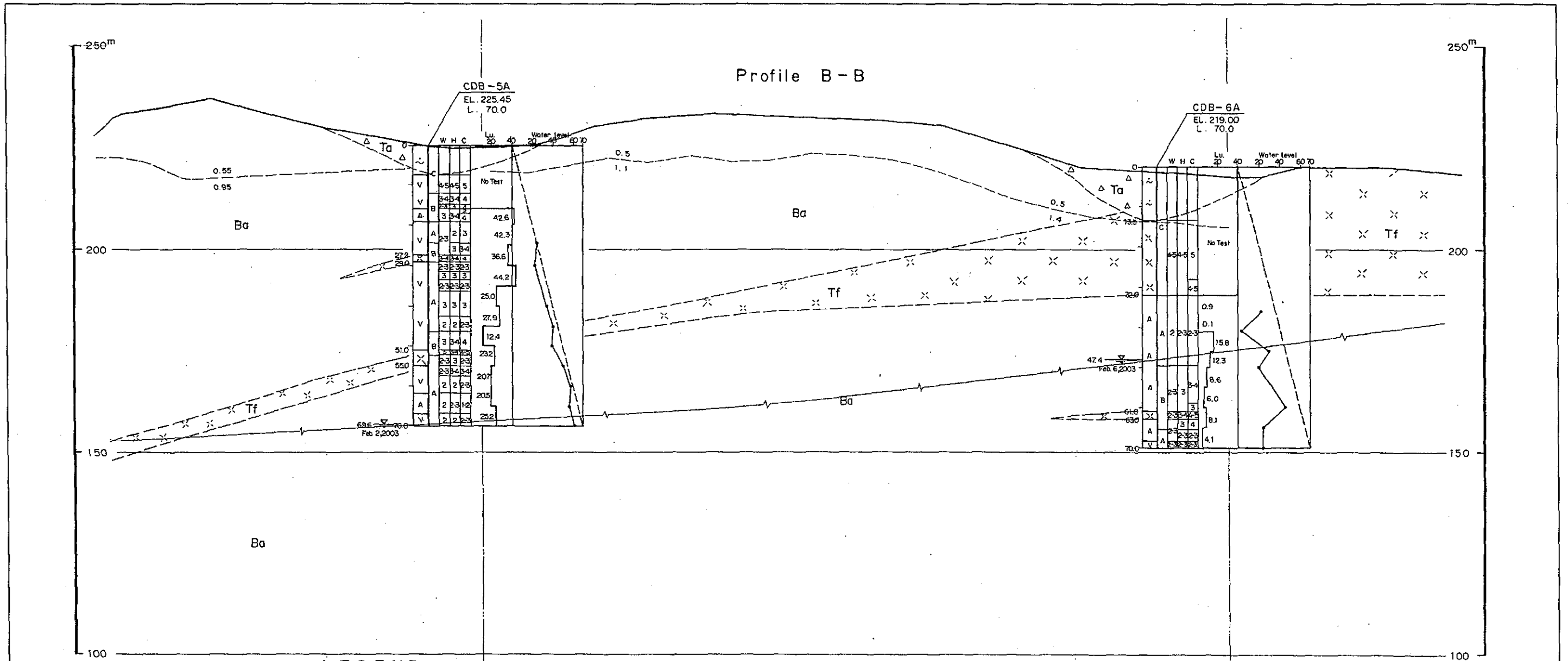
HARDNESS	CRACK SPACING								
	1	1-2	2	2-3	3	3-4	4	4-5	5
1									
1-2									
2		A Class Rockmass							
2-3									
3									
3-4		B Class Rockmass							
4									
4-5									
5			C Class Rockmass						

Standard of Rockmass Classification by J-Power for Drilled Core

CLASS	WEATHERING	HARDNESS	CRACK SPACING
1	Very fresh. No weathering of mineral component.	Very hard. Broken into knife-edged pieces by strong hammer blow.	over 30cm
2	Fresh. Some minerals are weathered slightly. Usually, no brown crack.	Hard. Broken into pieces by strong hammer blow.	10 to 30 cm
3	Fairly fresh. Some minerals are weathered. Cracks are stained and with weathered mineral.	Brittle. Broken into pieces by medium hammer blow.	5 to 10cm
4	Weathered. Fresh portions still remain partially.	Very brittle. Easily broken into pieces by slight hammer blow.	1 to 5cm
5	Strongly weathered. Most of minerals are weathered and altered to secondary minerals.	Soft. Able to dig with hammer.	under 1cm



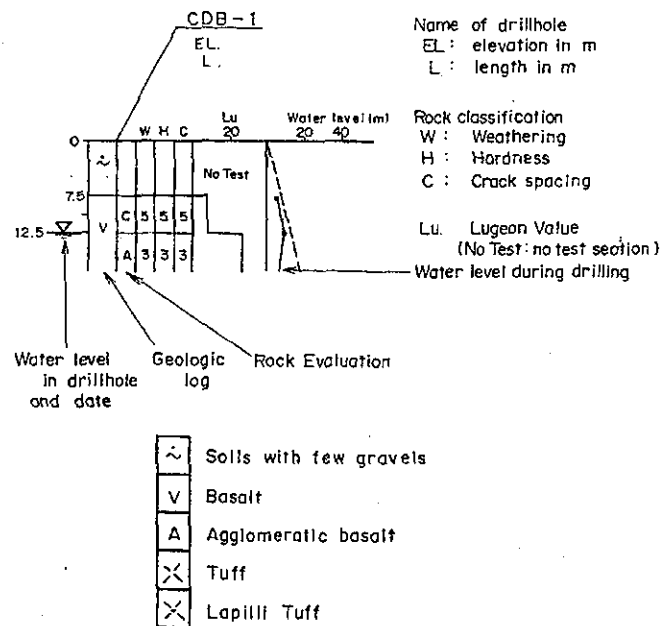
EL CHAPARRAL HYDROPOWER PROJECT
 GEOLOGICAL PROFILE OF DAM SITE
 Fig. 7.6



LEGEND

- Talus deposit and residual soil.
- Basalt
- Tuff
- Geologic boundary
- Groundwater table
- Velocity layers and their velocity (km/sec.)

(Log of Drillehole)

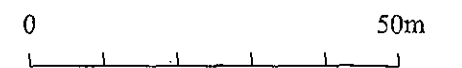


Standard of Rockmass Classification by J-Power for Drilled Core

CLASS	WEATHERING	HARDNESS	CRACK SPACING
1	Very fresh. No weathering of mineral component.	Very hard. Broken into knife-edged pieces by strong hammer blow.	over 30cm
2	Fresh. Some minerals are weathered slightly. Usually, no brown crack.	Hard. Broken into pieces by strong hammer blow.	10 to 30cm
3	Fairly fresh. Some minerals are weathered. Cracks are stained and with weathered mineral.	Brittle. Broken into pieces by medium hammer blow.	5 to 10cm
4	Weathered. Fresh portions still remain partially.	Very brittle. Easily broken into pieces by slight hammer blow.	1 to 5cm
5	Strongly weathered. Most of minerals are weathered and altered to secondary minerals.	Soft. Able to dig with hammer.	under 1cm

Standard of Rock Evaluation

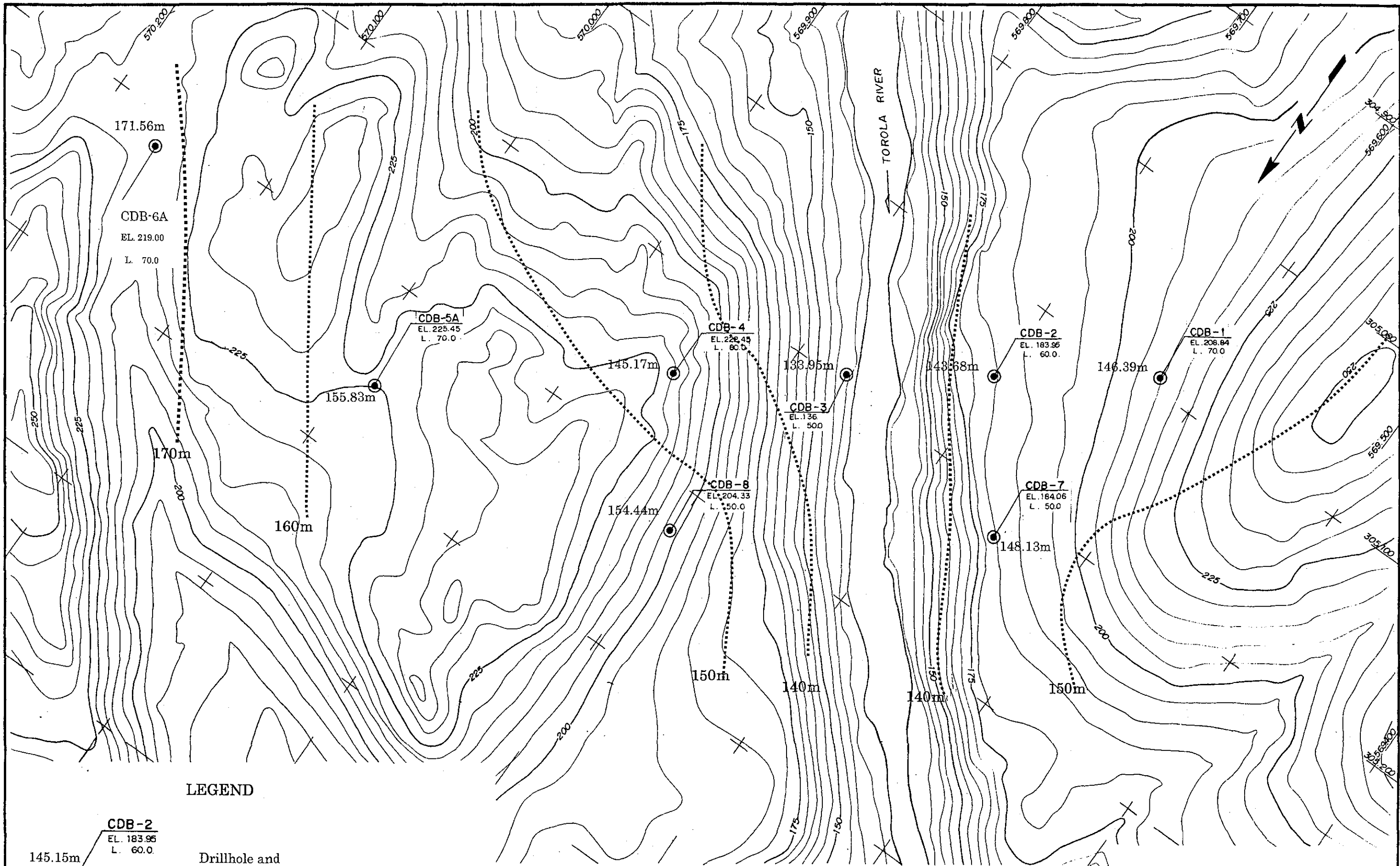
HARDNESS	CRACK SPACING				
	1	1-2	2	2-3	3
1					
1-2					
2	A Class Rockmass				
2-3					
3	B Class Rockmass				
3-4					
4	C Class Rockmass				
4-5					
5					



EL CHAPARRAL HYDROPOWER PROJECT
GEOLOGICAL PROFILE OF THE RIGHT BANK

Fig. 7.7

DATE



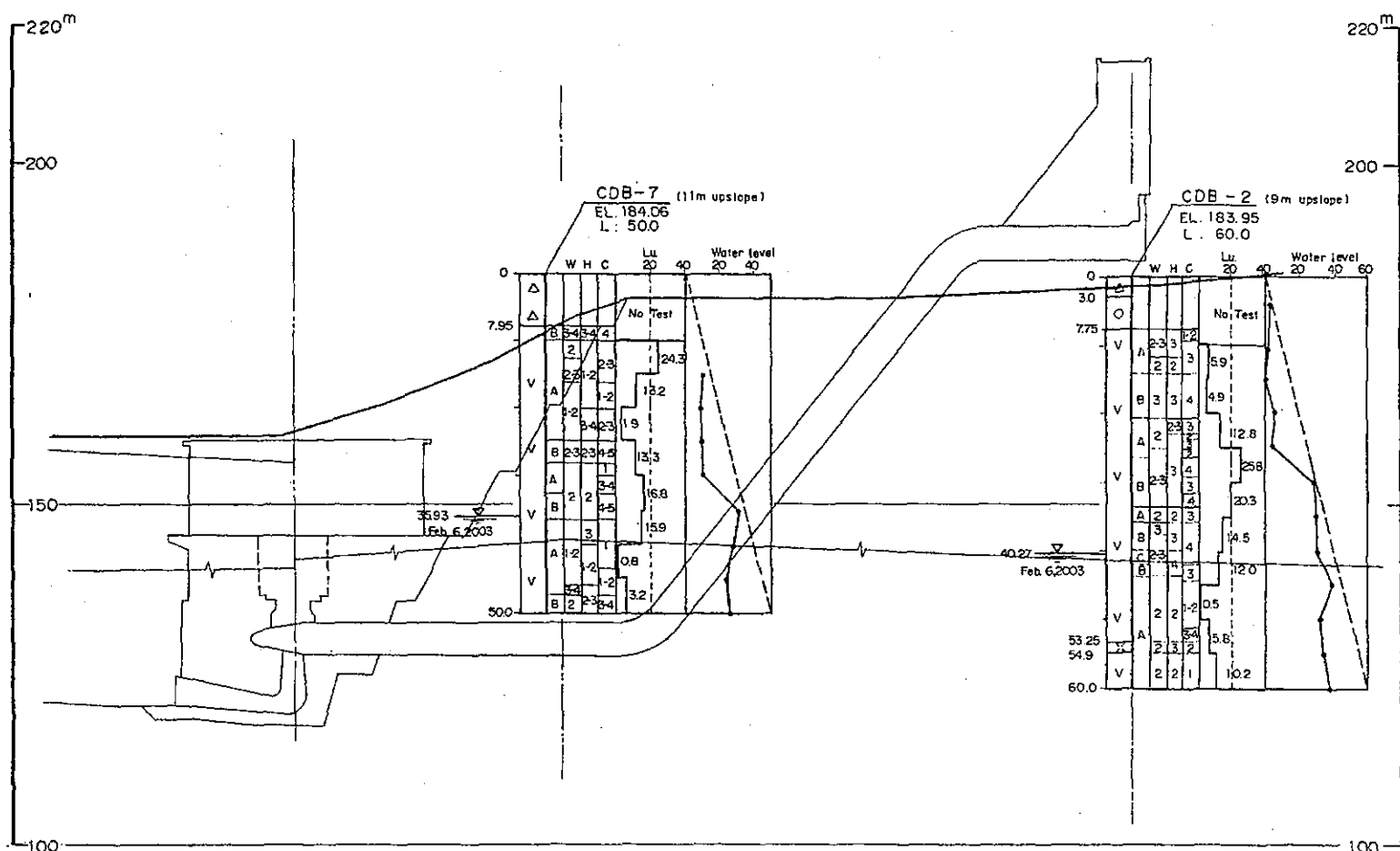
LEGEND

- CDB-2
 EL. 183.96
 L. 60.0
 Drillhole and its water level
- 150m
 Contour of groundwater table

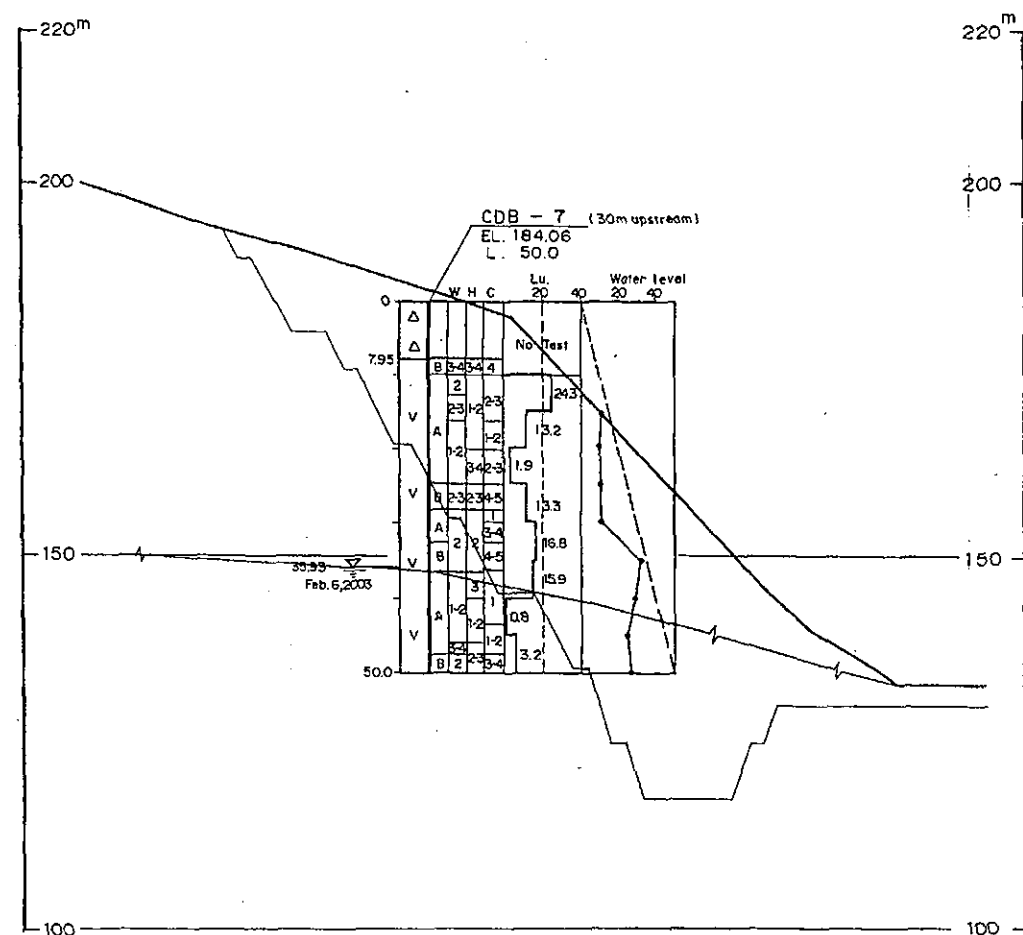


EL CHAPARRAL HYDROPOWER PROJECT
 GROUNDWATER TABLE AT DAM SITE
 Fig. 7.10 DATE

Profile C-C



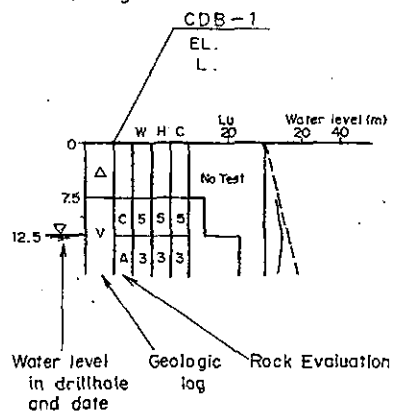
Profile D-D



LEGEND

- Talus deposit and residual soil.
- Basalt
- Tuff
- Geologic boundary
- Groundwater table
- Velocity layers and their velocity (km/sec)

(Log of Drillehole)



Name of drillhole
EL: elevation in m
L: length in m

Rock classification
W: Weathering
H: Hardness
C: Crack spacing

Lu: Lugeon Value
(No Test: no test section)
Water level during drilling

- Soils with angular gravels
- Soils with round gravels
- Basalt
- Agglomeratic basalt
- Tuff

Standard of Rockmass Classification by J-Power for Drilled Core

CLASS	WEATHERING	HARDNESS	CRACK SPACING
1	Very fresh. No weathering of mineral component.	Very hard. Broken into knife-edged pieces by strong hammer blow.	over 30cm
2	Fresh. Some minerals are weathered slightly. Usually, no brown crack.	Hard. Broken into pieces by strong hammer blow.	10 to 30cm
3	Fairly fresh. Some minerals are weathered. Cracks are stained and with weathered mineral.	Brittle. Broken into pieces by medium hammer blow.	5 to 10cm
4	Weathered. Fresh portions still remain partially.	Very brittle. Easily broken into pieces by slight hammer blow.	1 to 5cm
5	Strongly weathered. Most of minerals are weathered and altered to secondary minerals.	Soft. Able to dig with hammer.	under 1cm

Standard of Rock Evaluation

HARDNESS	CRACK SPACING				
	1	1-2	2	2-3	3
1					
1-2					
2	A Class Rockmass				
2-3					
3	B Class Rockmass				
3-4					
4	C Class Rockmass				
4-5					
5					

0 50m

EL CHAPARRAL HYDROPOWER PROJECT

GEOLOGICAL PROFILE OF POWER STATION SITE

Fig. 7.12

DATE

8. EARTHQUAKE

CONTENTS

8.	EARTHQUAKE.....	8-1
8.1	Outline.....	8-1
8.2	Seismic Activity.....	8-2
8.2.1	Seismic Activity in and around El Salvador.....	8-2
8.2.2	Historical Earthquakes around the Project Site.....	8-3
8.3	Seismic Risk Analysis.....	8-7
8.3.1	Seismic Risk Analysis based on Stochastic Technique.....	8-7
8.3.2	Presumption of Maximum Acceleration at the Project Site.....	8-9
8.3.3	Design Horizontal Seismic Coefficient.....	8-16

8. EARTHQUAKE

8.1 Outline

El Salvador is located on the Circum-Pacific Seismic Belt, a zone noted for frequent earthquake occurrence in the world. This country suffered many earthquake disasters in the past, and more recent earthquake disasters are given in Table 8.1. Since the project area is located in the area of high seismic activity, it is important to carry out sufficient evaluation and examination of the earthquake, and to carry out suitable consideration in the design of electric power facilities.

In this chapter, in order to make a basic study for the determination of the earthquake load to be used when designing the dam, --the main civil structure--, the seismic risk analysis based on the stochastic technique was performed. As a result of the estimation of the maximum acceleration value, the design seismic coefficient at the project site was set up.

Table 8.1 Recent Earthquake Disasters in El Salvador

Date	EPICENTER	Magnitude	Damage
6 May, 1951	Jucuapa y Chinameca	6.2	400 dead
3 May, 1965	San Salvador	6.0	125 dead; 4,000 houses destroyed
19 June, 1982	Pacific Ocean (Plate Subduction Zone)	7.0	8 dead
10 Oct, 1986	San Salvador	5.4	1,500 dead; 60,000 houses destroyed
13 Jan, 2001	Pacific Ocean (Plate Subduction Zone)	7.6	944 dead; 108,261 houses destroyed; 445 landslides
13 Feb, 2001	San Vicente	6.7	315 dead; 41,302 houses destroyed; 71 landslides

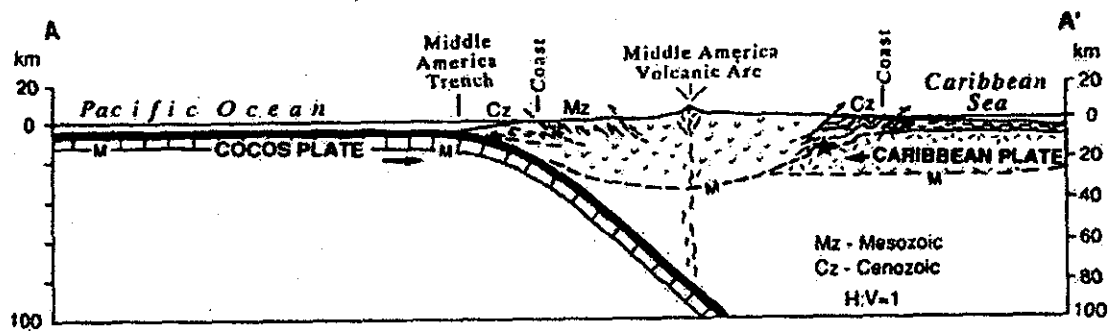
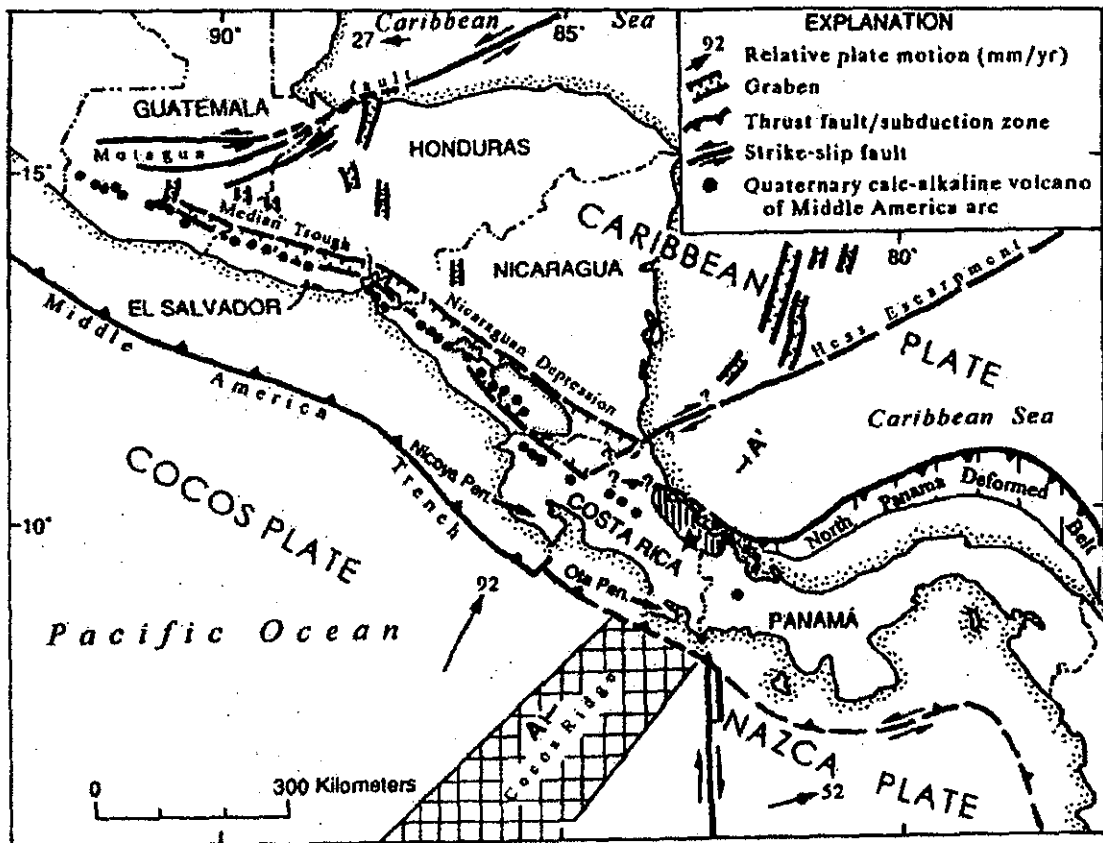
Source Book: *Cronología de sismos destructivos en El Salvador* : Centro de Investigaciones Geotécnicas(CIG, El Salvador)

8.2 Seismic Activity

8.2.1 Seismic Activity in and around El Salvador

In parallel to the coastal line of El Salvador lies the Central America Trench in the adjacent seas of the Pacific Ocean to the south of El Salvador. This trench is located on the boundary of the COCOS PLATE and the CARIBBEAN PLATE, and the COCOS PLATE sinks there in an acute angle at a comparatively high move speed (92mm/year) from the southwest to the northeast (Fig.8.1). The motion of this plate is the first cause for generating many earthquakes, and there is a possibility that a large-scale earthquake (magnitude of more than 8) will occur (the earthquake which occurred on January 13, 2001 belonged to this type).

In El Salvador, an active volcano belt is running from east to west. This volcanic activity is also considered to have been caused by the settlement of the plate. As this settlement prompted the earth's crust on the side of the Central America Trench to move secondarily, trenches and faults are formed, and this motion has become the second cause for generating earthquakes. This type of earthquakes (magnitude of less than 6.5) is smaller than the above-mentioned earthquakes in terms of energy scale. Because there is a possibility that this type of earthquakes will occur on the land with a shallow focus, large-sale shaking may take place locally, leading to serious damage.

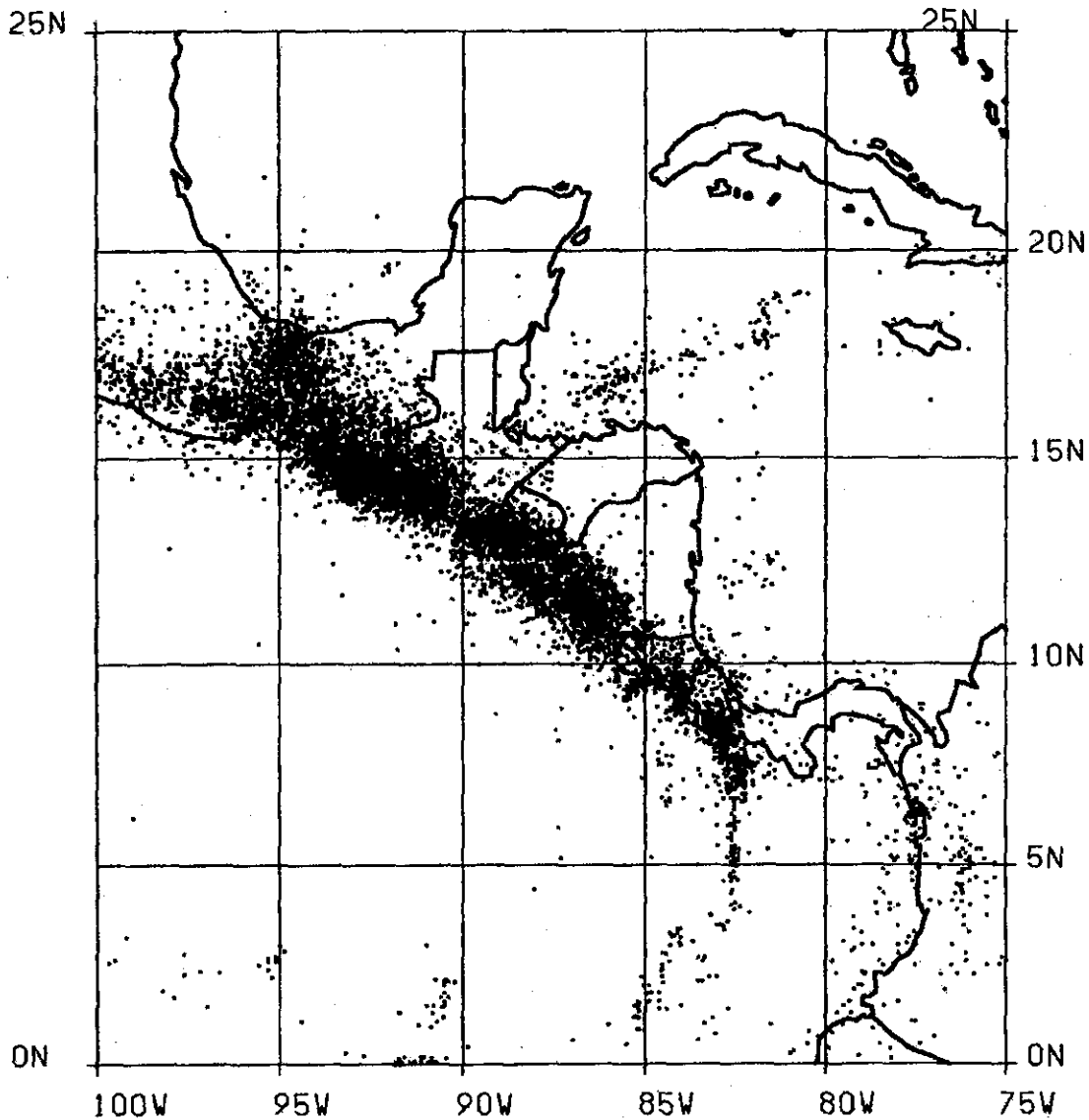


Source Book: *The January 13, 2001 Off the Coast of El Salvador Earthquake:*
Japan Society of Civil Engineers (JSCE)

Fig. 8.1 Seismo-Tectonics in Central-South America

8.2.2 Historical Earthquakes around the Project Site

The epicenters of earthquakes which occurred within a radius of 1,000 km of the project site during the past 100 years were obtained from the U.S. database (U.S. Department of the Interior, U.S. Geological Survey (USGS), National Oceanic & Atmospheric Administration (NOAA)) and are shown in Fig. 8.2



Source Book: U.S. Department of the Interior, U.S. Geological Survey (USGS),
National Oceanic & Atmospheric Administration (NOAA)

Fig.8.2 Epicenters of Historical Earthquakes around El Salvador (1902- 2002)

As is clear from the figure, earthquakes have occurred frequently on the boundary of the plates and in the land. Table 8.2 shows the earthquakes with magnitudes of more than 6.0 that occurred within a 200-km radius of the project site. Of these, the earthquake which recorded the maximum magnitude occurred on September 7, 1915 ($M_b=7.5$, depth = 80 km, epicentral distance = 71 km).

In recent years, two earthquakes -- one earthquake ($M_b=7.4$, depth = 60 km, epicentral distance = 97km) on January 13, 2001 and the other earthquake ($M_b=6.7$, depth = 10 km, epicentral distance = 66 km) on February 13-- brought about serious damage. The earthquake that occurred at the point closest to the project site took place on May8, 2001($M_b=6.3$, depth = 182 km, epicentral

distance = 41km). An earthquake with the hypocentral distance of 56 km, --the shortest hypocentral distance from the project site) occurred on May 8, 2001 (Mb=6.1).

Table 8.2 Historical Earthquakes around the Project Site

($D \leq 200$ km D: epicentral distance, magnitude ≥ 6.0)

Year	Month	Day	LONG	LAT	Magnitude	Epicentral Distance (km)	Depth (km)
1915	9	7	-89.00	14.00	7.5	71.3	80
1921	3	28	-87.50	12.50	7.1	177.4	30
1926	2	8	-89.00	13.00	7.0	118.8	30
1931	2	7	-87.00	13.00	6.1	175.5	100
1931	8	25	-89.50	12.50	6.0	195.8	30
1932	5	22	-90.00	14.20	6.3	181.5	80
1932	6	20	-89.00	12.50	6.3	166.7	80
1934	3	7	-87.70	13.20	6.4	102.2	30
1934	12	3	-88.70	15.00	6.4	130.7	30
1939	7	8	-88.00	12.50	6.0	156.1	90
1939	12	26	-88.20	13.20	6.3	75.7	75
1941	11	16	-88.50	13.20	6.1	75.5	80
1944	10	2	-89.70	14.50	6.6	161.4	160
1946	6	24	-89.00	14.70	6.3	115.5	260
1951	5	6	-87.80	13.00	6.6	113.3	30
1951	5	6	-87.80	13.00	6.4	113.3	96
1951	5	7	-87.80	13.00	6.3	113.3	30
1951	8	2	-87.80	13.00	6.1	113.3	33
1951	8	3	-87.80	13.00	6.3	113.3	33
1951	8	3	-87.80	13.00	6.0	113.3	33
1954		19	-87.50	12.50	6.7	177.4	30
1955		4	-87.00	13.00	6.4	175.5	30
1955	4	26	-89.50	13.50	6.6	130.3	60
1958	6	27	-88.50	13.00	6.3	97.3	60
1959	5	3	-87.50	12.50	6.0	177.4	100
1961	4	12	-88.90	13.20	6.2	94.5	122
1961	5	23	-87.30	12.70	6.6	172.5	138
1976	2	4	-89.10	15.32	7.2	179.3	5
1976	2	8	-88.47	15.57	6.0	188.4	5
1978	5	31	-87.17	12.77	6.5	177.3	76
1978	12	6	-89.63	13.15	6.4	159.4	33
1982	1	12	-87.58	13.17	6.4	113.8	6
1982	6	19	-89.33	13.32	7.0	122.1	81

Year	Month	Day	LONG	LAT	Magnitude	Epicentral Distance (km)	Depth (km)
1982	7	2	-89.28	13.07	6.2	134.2	64
1983	7	18	-87.18	12.67	6.0	183.8	86
1985	10	12	-89.72	13.15	6.2	167.2	41
1986	10	10	-89.12	13.83	6.0	82.4	7
1993	6	12	-87.53	13.25	6.2	112.0	217
1995	5	21	-87.93	12.13	6.0	197.2	51
1995	6	14	-88.37	12.13	6.7	191.9	25
1996	7	22	-88.72	13.08	6.0	95.2	61
1996	12	10	-88.93	12.52	6.0	162.1	33
1996	12	14	-88.78	12.73	6.1	133.8	33
1996	12	17	-88.92	12.47	6.0	166.5	33
1996	12	19	-89.97	13.05	6.0	196.9	33
1997	5	15	-89.78	14.47	6.0	168.0	274
1997	8	24	-89.58	13.55	6.0	137.3	139
1997	11	9	-88.82	13.85	6.6	50.0	176
1997	12	18	-88.73	13.83	6.3	41.1	182
1999	4	3	-87.63	13.17	6.3	109.9	38
2001	1	13	-88.67	13.05	7.4	96.6	60
2001	1	14	-88.58	13.12	6.1	86.7	48
2001	1	15	-88.78	13.18	6.0	88.8	67
2001	1	15	-88.58	13.08	6.2	90.2	74
2001	1	16	-88.60	13.02	6.1	97.8	44
2001	1	16	-88.70	12.98	6.1	104.8	62
2001	1	25	-88.88	12.92	6.0	119.8	33
2001	2	2	-88.97	12.82	6.1	133.9	54
2001	2	7	-88.93	13.22	6.2	95.4	63
2001	2	13	-88.93	13.67	6.7	66.4	10
2001	2	17	-88.92	13.07	6.0	107.6	33
2001	2	28	-88.83	13.28	6.3	82.8	65
2001	3	16	-88.70	13.13	6.2	89.4	48
2001	3	18	-87.40	12.53	6.1	180.3	95
2001	3	29	-88.93	13.08	6.2	107.1	33
2001	5	8	-88.78	13.60	6.1	55.0	10
2001	7	7	-87.52	12.43	6.0	182.8	79
2001	9	18	-88.77	12.98	6.0	107.6	62

8.3 Seismic Risk Analysis

8.3.1 Seismic Risk Analysis based on Stochastic Technique

(1) Outline of Analysis

In this chapter, the maximum acceleration at the project site was estimated based on the data of historical earthquakes by a stochastic technique, and this, upon statistical reprocessing, was used to derive a maximum acceleration which may be expected in any return period.

Furthermore, the value of the design seismic coefficient used for the dam stability analysis was set up from the calculated maximum acceleration value.

It should be noted that there is another evaluation method for the seismic risk analysis, -- the deterministic technique. This is a method in which the earthquake motion assumable for a site is estimated using numerical analysis, through establishing fault models for earthquakes based on the seismic activity, distribution of earthquake faults, and crustal movements while simultaneously taking into account the underground structure.

This method can lead to a rational result when conditions required for the analysis can be set up correctly. However, it is difficult to estimate fault parameters or underground structures in many cases; therefore, this method cannot be a generally applicable method.

In contrast, the stochastic technique has good reliability when enough earthquake data are available and is the generally used method at present. Therefore, it was decided that the stochastic technique should be used in the seismic risk analysis.

(2) Earthquake Data

The U.S. database (U.S. Geological Survey (USGS), National Oceanic & Atmospheric Administration (NOAA)) contains long-term earthquake data, and these were used for the seismic risk analysis.

The earthquakes that occurred within a radius of 1,000 km of the project site during the period between 1902 and 2002 number 9,357 in total. Table 8.3 shows the annual number of earthquakes in that period. The project site is located at longitude 88°21'16" west and latitude 13°52'03" north. Table 8.4 shows the distribution of magnitudes and of epicentral distances of the earthquakes.

A radius of 1,000 km was used here as the object of evaluation, as it is considered appropriate for evaluation when the damping characteristics of acceleration of earthquake motion is considered.

The number of earthquakes available for the study was considered appropriate to serve as the fundamental data for the stochastic technique in light of the number and scale of earthquakes that have taken place.

Table 8.3 Annual Number of Earthquakes in the 1902-to-2002 Period

($D \leq 1,000$ km, D: epicentral distance)

YEAR	N	SUM OF N	YEAR	N	SUM OF N
1902	4	4	1957	16	277
1904	2	6	1958	11	288
1907	1	7	1959	22	310
1909	1	8	1960	12	322
1910	2	10	1961	18	340
1911	1	11	1962	12	352
1912	2	13	1963	119	471
1913	1	14	1964	197	668
1914	2	16	1965	203	871
1915	2	18	1966	209	1080
1916	7	25	1967	184	1264
1917	1	26	1968	127	1391
1919	4	30	1969	106	1497
1920	1	31	1970	167	1664
1921	4	35	1971	86	1750
1924	2	37	1972	112	1862
1925	2	39	1973	100	1962
1926	6	45	1974	118	2080
1928	6	51	1975	108	2188
1929	1	52	1976	136	2324
1931	17	69	1977	98	2422
1932	7	76	1978	155	2577
1933	9	85	1979	160	2737
1934	14	99	1980	135	2872
1935	5	104	1981	102	2974
1936	2	106	1982	174	3148
1937	9	115	1983	177	3325
1938	1	116	1984	148	3473
1939	11	127	1985	169	3642
1940	4	131	1986	147	3789
1941	10	141	1987	176	3965
1942	7	148	1988	207	4172
1943	5	153	1989	142	4314
1944	5	158	1990	166	4480
1945	4	162	1991	212	4692
1946	9	171	1992	369	5061
1947	3	174	1993	422	5483
1948	3	177	1994	215	5698
1949	3	180	1995	278	5976
1950	12	192	1996	319	6295
1951	14	206	1997	345	6640
1952	12	218	1998	474	7114
1953	7	225	1999	498	7612
1954	13	238	2000	525	8137
1955	11	249	2001	627	8764
1956	12	261	2002	593	9357

**Table 8.4 Distribution of Magnitudes and Epicentral Distances
in the 1902-to-2002 Period**

	0<=D<50	<100	<200	<300	<400	<500	<600	<700	<800	<1000	1000<=	TOTAL
0<M<3	0	0	0	0	0	0	0	0	0	0	0	0
<3.5	1	0	3	12	8	9	10	9	13	15	0	80
<4.0	6	22	59	100	107	91	88	65	64	97	0	699
<4.5	22	105	400	432	392	333	297	186	157	226	0	2550
<5.0	17	72	393	464	439	333	276	224	234	497	0	2949
<5.5	10	51	166	185	212	233	235	226	319	471	0	2108
<6.0	0	7	59	61	77	67	41	44	41	60	0	457
<6.5	1	13	31	39	63	49	26	27	9	55	0	313
<7.0	1	1	8	19	28	10	12	15	16	28	0	138
<7.5	0	3	4	7	4	8	7	2	1	19	0	55
<8.0	0	0	0	4	0	0	2	0	0	2	0	8
8.0<=	0	0	0	0	0	0	0	0	0	0	0	0
TOTAL	58	274	1123	1323	1330	1133	994	798	854	1470	0	9357

D : EPICENTRAL DISTANCE (KM)

M : MAGNITUDE

8.3.2 Presumption of Maximum Acceleration at the Project Site

(1) Analysis of Maximum Acceleration

In order to estimate the maximum acceleration at the project site using the earthquakes data, five attenuation formulas below, which give the maximum acceleration based on the magnitude and epicentral distance, were used.

These formulas were drawn by the analysis based on the survey data for hard rock. These were selected from among many other formulas, because these are frequently used for the estimation of earthquake response of foundation rock at the dam site.

- 1) Proposed by C. Oliveira
 $\log A = 3.09 + 0.347M - 2.0 \log(R+25)$
- 2) Proposed by R. K. McGuire
 $\log A = 2.674 + 0.278 M - 1.301 \log(R+25)$
- 3) Proposed by L. Esteva and E. Rosenblueth
 $\log A = 2.041 + 0.347 M - 1.6 \log(R)$
- 4) Proposed by Katayama
 $\log A = 2.308 + 0.411 M - 1.637 \log(R+30)$
- 5) Proposed by Okamoto
 $\log (A/640) = (\Delta+40)(-7.6 + 1.724 M - 0.1036 M^2)/100$

Where:

A : Acceleration value (gal)

M : Magnitude

Δ : Epicentral distance (km)

R : Hypocentral distance (km)

Maximum accelerations were calculated for each earthquake by using the five formulas.

Table 8.5 shows annual maximum accelerations calculated by these five formulas.

Table 8.5 Annual Maximum Acceleration in the 1902-to-2002 Period (gal)

Year	Attenuation model				
	Oliveira	McGuire	Esteva	KATAYAMA	OKAMOTO
1902	6.07	37.80	6.17	24.56	19.05
1904	0.80	10.13	1.12	4.76	0.05
1907	3.18	22.85	3.27	11.84	6.05
1909	0.78	9.09	0.99	3.72	0.06
1910	1.18	12.27	1.44	5.62	0.33
1911	0.32	4.93	0.46	1.68	0.00
1912	1.92	15.96	2.06	7.29	1.38
1913	0.57	6.99	0.71	2.49	0.01
1914	1.22	12.56	1.49	5.79	0.48
1915	27.76	98.62	24.47	76.51	175.52
1916	4.49	29.47	4.53	16.86	12.89
1917	0.47	6.79	0.68	2.73	0.00
1919	4.39	27.20	4.22	14.04	13.37
1920	0.81	8.58	0.93	3.12	0.04
1921	8.52	43.69	7.88	26.59	34.03
1924	0.66	8.10	0.85	3.19	0.02
1925	1.42	13.06	1.59	5.66	0.72
1926	14.82	61.65	13.13	39.67	66.14
1928	0.51	7.12	0.72	2.85	0.01
1929	0.24	3.85	0.33	1.15	0.00
1931	3.17	20.43	2.99	8.93	6.23
1932	4.22	26.18	3.97	13.60	11.45
1933	1.08	10.00	1.15	3.64	0.10
1934	12.21	50.98	10.76	28.80	46.89
1935	1.53	14.31	1.77	6.68	0.78
1936	0.94	9.16	1.03	3.27	0.06
1937	1.40	11.77	1.43	4.42	0.34
1938	0.27	4.02	0.35	1.16	0.00
1939	10.74	46.01	9.46	24.75	64.19
1940	1.89	15.72	2.02	7.12	1.52
1941	8.97	40.16	7.91	20.42	53.46
1942	6.05	37.73	6.15	24.50	19.05
1943	1.91	15.85	2.04	7.20	1.52
1944	3.77	24.21	3.64	11.88	20.86
1945	4.97	29.52	4.72	15.53	13.04
1946	2.51	18.57	2.54	8.56	29.09
1947	2.89	21.47	3.01	10.96	8.81
1948	0.61	7.69	0.80	2.99	0.02
1949	1.29	11.59	1.38	4.54	0.34
1950	2.66	19.11	2.65	8.97	2.96
1951	11.87	51.05	10.50	29.64	47.26
1952	4.02	24.74	3.79	11.90	7.54
1953	3.52	22.26	3.32	10.19	5.15
1954	6.09	33.39	5.63	17.87	18.25
1955	8.46	40.95	7.60	22.66	35.39
1956	3.74	25.58	3.79	13.74	8.78
1957	1.47	12.63	1.55	5.06	0.83
1958	9.58	42.72	8.46	22.62	41.83
1959	4.71	25.73	4.24	11.45	8.15
1960	1.37	11.17	1.35	4.34	0.29
1961	5.42	29.22	4.91	14.04	39.71
1962	2.88	17.94	2.63	6.97	2.44
1963	2.26	13.16	1.99	4.27	3.08
1964	3.47	19.68	3.12	8.11	10.28
1965	3.84	20.44	3.39	7.57	3.53
1966	6.93	25.98	7.26	10.20	50.35
1967	4.73	21.27	4.30	6.90	8.92
1968	18.94	52.44	28.48	19.74	51.79
1969	8.35	30.78	8.42	10.68	24.80
1970	2.94	17.38	2.63	6.91	27.18
1971	4.67	24.07	4.12	9.71	24.37
1972	7.80	33.63	6.91	14.55	25.07
1973	2.31	14.71	2.09	5.07	2.87
1974	9.63	40.65	8.49	19.75	36.21
1975	3.13	16.64	2.75	5.37	2.20
1976	12.72	47.66	13.20	30.22	81.36
1977	6.66	29.62	5.90	12.06	41.88
1978	5.85	31.48	5.33	15.92	15.54
1979	5.28	23.96	4.71	11.24	10.25
1980	4.23	26.48	4.07	13.52	9.28
1981	4.61	21.30	4.15	7.69	6.69
1982	11.23	51.67	10.85	32.14	65.11
1983	2.86	18.81	2.70	7.92	3.90
1984	3.87	20.07	3.41	7.28	25.97
1985	7.14	29.52	6.50	11.51	16.48
1986	12.50	48.93	11.07	25.26	37.73
1987	10.36	37.62	10.00	14.89	40.24
1988	3.47	18.83	3.07	8.29	3.97
1989	4.12	22.20	3.66	8.80	6.69
1990	4.91	25.63	4.36	10.93	7.62
1991	6.45	26.03	6.14	8.80	13.91
1992	4.48	28.97	4.46	16.18	12.40
1993	3.55	21.40	3.26	9.13	28.54
1994	7.30	30.06	6.65	12.08	17.82
1995	5.27	30.33	4.94	15.83	13.89
1996	7.98	36.81	7.04	18.09	30.71
1997	6.04	31.12	6.22	16.19	138.55
1998	5.02	26.42	4.47	11.59	16.12
1999	11.55	44.41	10.37	22.11	36.62
2000	5.80	29.03	5.14	13.00	14.90
2001	35.15	93.29	90.12	66.34	125.66
2002	6.69	27.03	6.65	10.71	16.11

(2) Statistical Analysis

The relationship between the maximum acceleration and the return period was derived by estimating the stochastic functions based on the maximum accelerations calculated earlier. Gumbel's extreme value theory was used for estimating the stochastic functions. The theory can be applied even when the original distribution of the stochastic variables is unknown, and it allows the estimation and evaluation of the frequency of earthquake occurrence and the return period if hypothetical conditions are satisfied.

Since it is presumed that there is an upper limit to the maximum amplitude of earthquake motion at any site, the use of the third asymptotic distribution, which assumes that there is an upper limit, has been judged to be reasonable. The third asymptotic distribution is expressed by the following formula.

$$P_n(x) = \exp\left\{-\frac{(W-x)}{(W-U)}\right\} \cdot k$$

Where:

x : random stochastic variable

$$x = \log A_{max}$$

A_{max} : maximum acceleration of earthquake motion at a certain site
in a unit period of time

W : upper limit of maximum amplitude

U : maximum value of characteristic

k : shape factor

Fig. 8.3 to 8.7 shows the stochastic function which shows the relation between the maximum acceleration and the return period calculated by each attenuation formula.

Two asymptotic lines were drawn on the same graph. The first line was drawn in an usual way, and the second line was drawn so as to exceed the maximum acceleration value in an attempt to keep the estimated acceleration value from not falling below the keyed-in historical data. Consequently, the second line was selected because it yielded greater acceleration values.

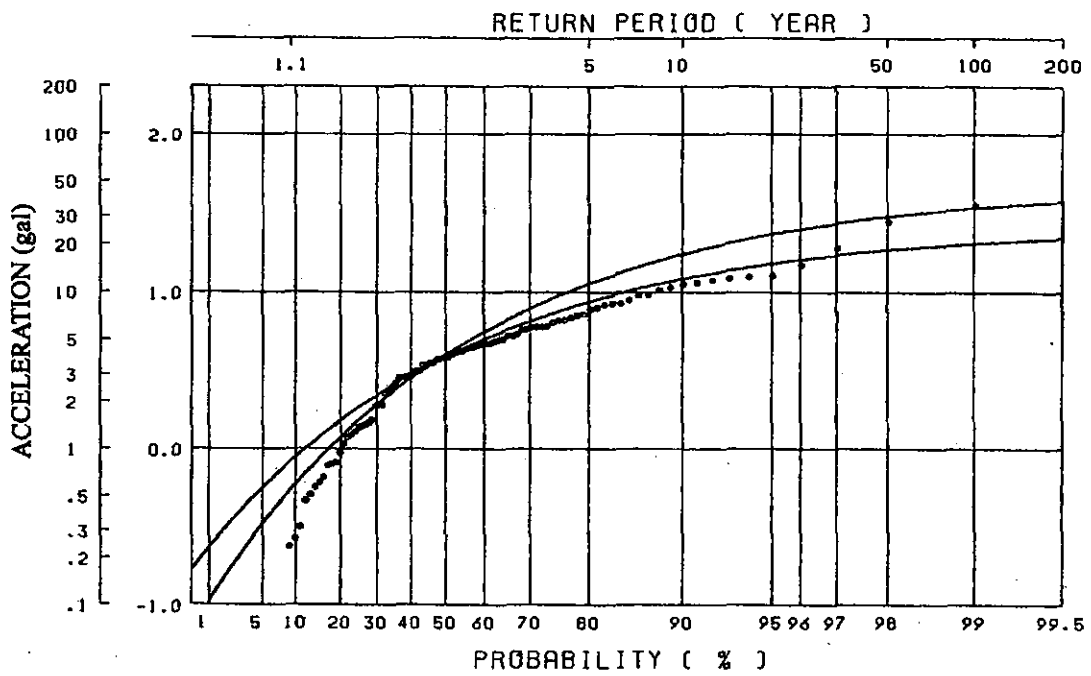


Fig.8.3 Return Period for Maximum Acceleration Calculated based on the Equation of C. Oliveira

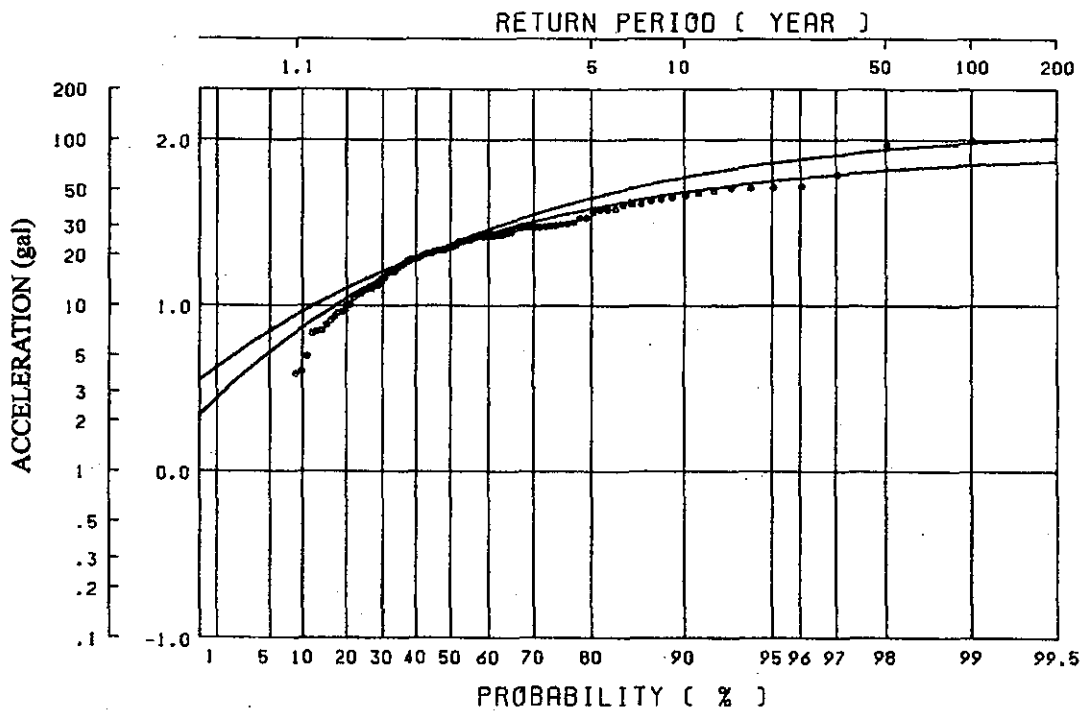


Fig.8.4 Return Period for Maximum Acceleration as Calculated by the Equation of P. K. McGuire

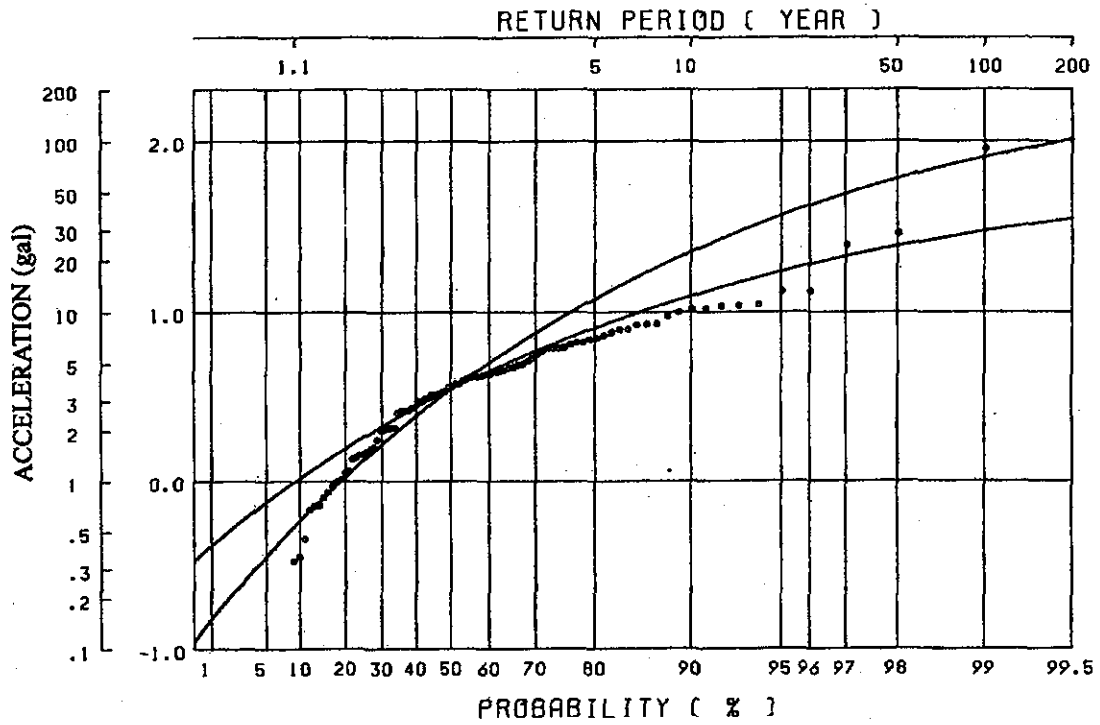


Fig.8.5 Return Period for Maximum Acceleration as Calculated by the equation of L. Esteva and E. Rosenbluth

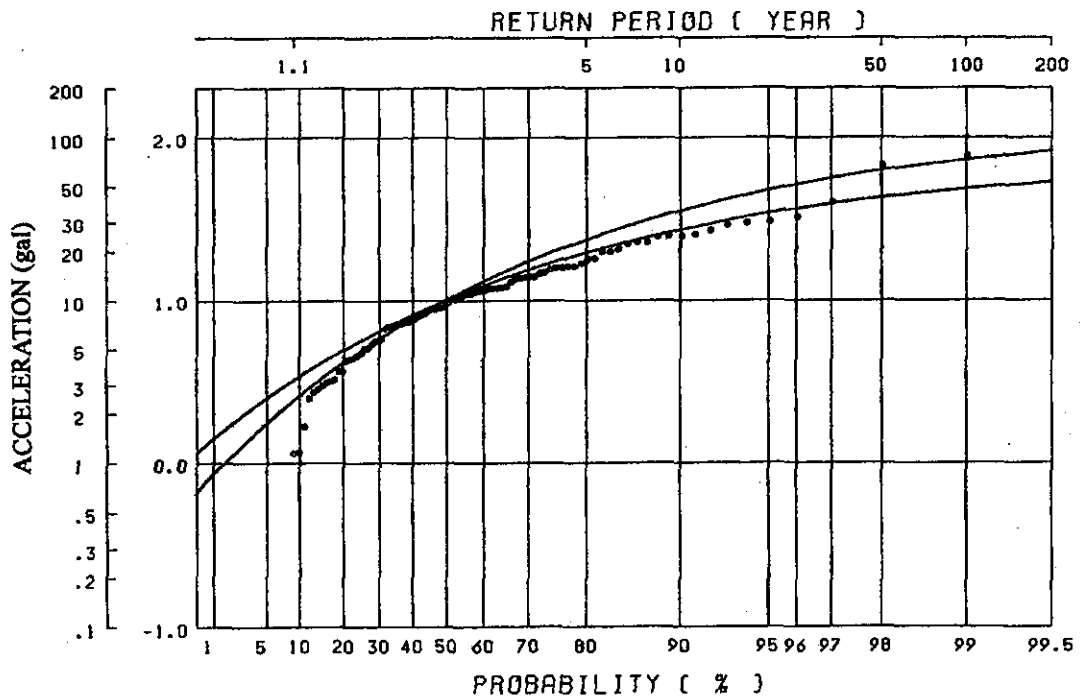
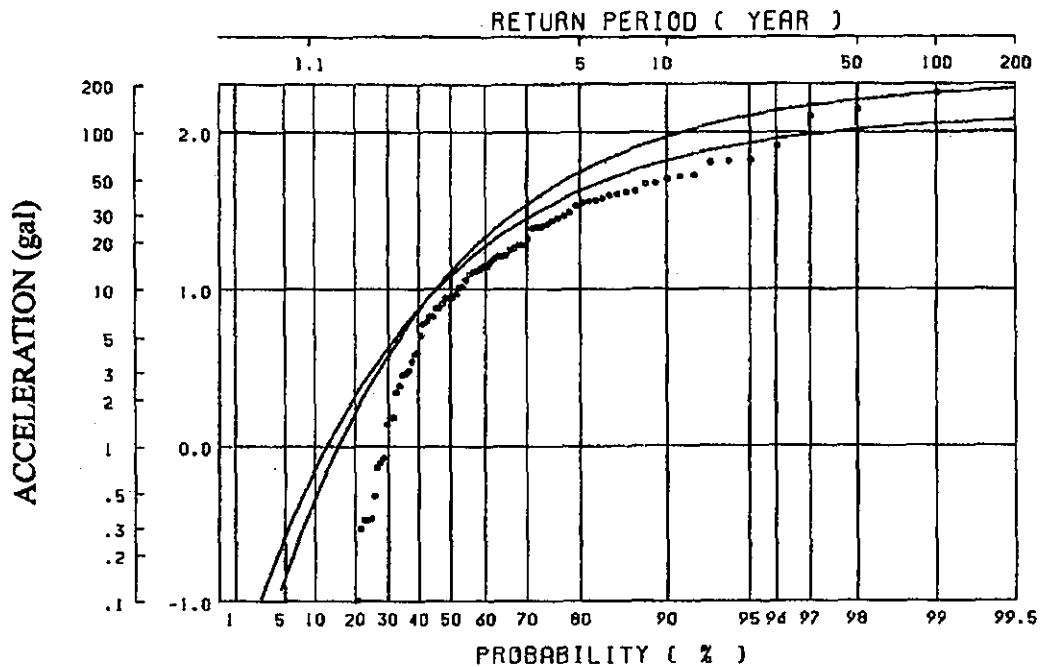


Fig.8.6 Return Period for Maximum Acceleration as Calculated by the Equation of T. Katayama



$$S: \text{LOG}(A/640) = [D+40](-7.6+1.724H-0.1036M^{**2})/100$$

(S. OKAMOTO)

Fig.8.7 Return Period for Maximum Acceleration as Calculated by the Equation of S. Okamoto

(3) Maximum Acceleration for Design

Table 8.6 shows the maximum acceleration that was estimated for each return period at the project site. It is understood that there is a big difference in the values of the estimated maximum acceleration based on each attenuation formula.

Table 8.6 Maximum Accelerations for Eight Return Periods

[The asymptotic line exceeds the average value]

Attenuation Model	Return Period (Year)							
	50	100	150	200	300	500	1000	10000
①Oliveira	18.58	20.51	21.44	22.01	22.72	23.46	24.23	25.60
②McGuire	65.66	70.85	73.37	74.95	76.92	79.00	81.25	85.47
③Esteva	24.23	29.64	32.77	34.96	37.97	41.61	46.21	58.31
④KATAYAMA	42.53	48.15	51.09	53.02	55.51	58.31	61.53	68.46
⑤OKAMOTO	103.77	112.94	116.86	119.13	121.72	124.18	126.48	129.64

[The asymptotic line exceeds the value of the greatest data]

Attenuation Model	Return Period (Year)							
	50	100	150	200	300	500	1000	10000
①Oliveira	30.14	34.25	36.27	37.53	39.09	40.73	42.48	45.61
②McGuire	87.55	96.38	100.73	103.47	106.90	110.57	114.55	122.12
③Esteva	60.03	80.81	93.72	103.09	116.44	133.26	155.54	219.14
④KATAYAMA	62.46	73.06	78.73	82.49	87.43	93.02	99.54	113.89
⑤OKAMOTO	159.36	176.01	183.19	187.36	192.14	196.71	200.99	206.89

Each attenuation formula is drawn from the analysis based on the actual survey data, and the estimated maximum acceleration values from the formulas differ depending on geological conditions. Given the high seismic activity in El Salvador, it has been judged appropriate estimate an acceleration value enveloping the results obtained here for the design work. Therefore, 220 gal was adopted as the maximum acceleration for design.

8.3.3 Design Horizontal Seismic Coefficient

Generally, the relationship between the maximum horizontal acceleration of earthquake motion and the design horizontal seismic coefficient is expressed as follows.

$$K_h = R \times (A_{max} / 980)$$

Where:

K_h : design horizontal seismic coefficient

R : conversion factor

A_{max} : maximum acceleration of earthquake motion (gal)

The design horizontal seismic coefficient is called the effective or equivalent seismic coefficient. The equivalent seismic coefficient was set up so that the largeness of stresses produced in structures by earthquake motion during the dynamic analysis would equal the one during the static analysis. As for the conversion factor, the formula below has been proposed in Japan.

$$K_h = (0.40 \sim 0.60) \times (A_{max} / 980)$$

The conversion factor changes with the frequency characteristic of earthquake motion and ground conditions, and it will be decided after examining these characteristics. Since the project site is located in the area where earthquakes occur frequently, the conversion factor of 0.6 was adopted as a conservative value. The design horizontal seismic coefficient was calculated to be 0.135, based on which 0.15 was adopted as a conservative value.

At the Feasibility Design stage, the static coefficient method was adopted for design work. However, at the stage of Detailed Design, it is desirable to carry out dynamic analysis in consideration of the dynamic characteristic of the dam and ground foundations during earthquake motion and to re-evaluate the results of the static analysis based on the dynamic results.

